

AUGUST 2000



INSPECTION CITY INSPECTED 4

20000925 147

Naval Air Warfare Center Weapons Division

FOREWORD

This report summarizes work performed at the Naval Air Warfare Center Weapons Division (NAWCWD), China Lake, California, to investigate the acoustic combustion instability response of tactical solid rocket motors to acoustic pulsing. In particular, effects of chamber pressure, pulse amplitude, and propellant were addressed. This report contains experimental data from 10 solid rocket motor firings performed from 1994 through 1997. A key important finding was the adverse effect raising the combustion chamber pressure had on a motor's susceptibility to experience combustion instability. The higher the pressure the more likely combustion instability will occur. A second finding was the bracketing of the pulse amplitude required to force a motor into combustion instability. This report contains information on the motors fired, propellants used, laboratory scale data, pulsing details, motor instrumentation, amplitude analysis, and frequency analysis.

Approved by
JOHN W. FISCHER, *Head*
Research & Technology Department
22 August 2000

Under authority of
C. H. JOHNSTON
RADM, U.S. Navy
Commander

Released for publication by
K. L. HIGGINS
Director for Research and Engineering

NAWCWD Technical Publication 8444

Published by Technical Information Division
Collation Cover, 24 leaves
First printing 85 copies

REPORT DOCUMENTATION PAGE			Form Approved OMB No. 0704-0188	
Public reporting burden for this collection of information is estimated to average 1 hour per response, including the time for reviewing instructions, searching existing data sources, gathering and maintaining the data needed, and completing and reviewing the collection of information. Send comments regarding this burden estimate or any other aspect of this collection of information, including suggestions for reducing this burden, to Washington Headquarters Services, Directorate for Information Operations and Reports, 1215 Jefferson Davis Highway, Suite 1204, Arlington, VA 22202-4302, and to the Office of Management and Budget, Paperwork Reduction Project (0704-0188), Washington, D.C. 20503.				
1. AGENCY USE ONLY (Leave Blank)		2. REPORT DATE		3. REPORT TYPE AND DATES COVERED
		August 2000		Final report, 1998
4. TITLE AND SUBTITLE			5. FUNDING NUMBERS	
Pulsed Motor Firings (U)				
6. AUTHOR(S)				
Fred S. Blomshield				
7. PERFORMING ORGANIZATION NAME(S) AND ADDRESS(ES)			8. PERFORMING ORGANIZATION REPORT NUMBER	
Naval Air Warfare Center Weapons Division China Lake, CA 93555-6100			NAWCWD TP 8444	
9. SPONSORING/MONITORING AGENCY NAME(S) AND ADDRESS(ES)			10. SPONSORING/MONITORING AGENCY REPORT NUMBER	
11. SUPPLEMENTARY NOTES				
12a. DISTRIBUTION/AVAILABILITY STATEMENT			12b. DISTRIBUTION CODE	
Approved for public release; distribution is unlimited.				
13. ABSTRACT (Maximum 200 words)				
See reverse.				
14. SUBJECT TERMS			15. NUMBER OF PAGES	
combustion instability			46	
pulsed motors				
tangential mode				
solid rockets				
stability additives				
longitudinal mode				
solid propellant				
non-linear				
			16. PRICE CODE	
17. SECURITY CLASSIFICATION OF REPORT	18. SECURITY CLASSIFICATION OF ABSTRACT	19. SECURITY CLASSIFICATION OF THIS PAGE	20. LIMITATION OF ABSTRACT	
UNCLASSIFIED	UNCLASSIFIED	UNCLASSIFIED	SAR	

13. ABSTRACT

(U) Combustion stability additives like zirconium carbide (ZrC), aluminum oxide (Al₂O₃), and zirconium ortho-silicate (ZrSiO₄) have long been known to suppress combustion instability in reduced smoke, composite propellant solid rocket systems. Often, as little as 0.5% additive can stabilize an otherwise unstable rocket motor. The additives appear to have effects on both linear and nonlinear pulsed instabilities. Although several theories have been proposed, the actual mechanism on how stability additives work remains unknown. The common belief that additive particle damping alone stabilizes rocket motors is not true. Somehow, the additives change the response behavior of the propellant. Past studies have shown that the additive effect is a combination of particle damping and a reduction in the combustion response of the propellant. In the past study, four propellants were studied containing 0, 1, 3, and 5% ZrC. In this study, the 3% propellant used before will be used again, except 3% HMX will be used in one formulation and 3% ultra fine aluminum or ALEX will be used in another. The emphasis here is to examine the combustion response changes. This paper will present the results of T-burner response testing and compare the results to past propellants containing additives. The reason for the work is that recent evidence suggests that traditional additives may not work as well when solid motors are operating at higher pressures. In addition, additives like the ones proposed, add energy to the propellant which would be a performance advantage over classical additives like ZrC.

CONTENTS

Acknowledgments	1
Abstract	3
Introduction	3
Motor Firings Details	7
Firing Results and Analysis of Motors No. 3 Through 5	12
Firing Results and Analysis of Motors No. 6 Through 10	27
Conclusions	42
References	44

ACKNOWLEDGMENTS

The author wishes to thank Jay Levine of the Phillips Laboratory, Edwards Air Force Base, for his help in interpreting the nonlinear modeling results and Bob Beddini of the University of Illinois for his help in understanding acoustic boundary layers. The author also thanks Richard Hoery and Richard Stalnaker of the Naval Air Warfare Center for their help in building, instrumenting, and firing the motors. Their abilities and insight were greatly appreciated. The author also wishes to thank Scott Fuller, Fred Zarlingo, and Tom Loftus of the Naval Air Warfare Center for supporting this effort. An atmosphere has been established allowing full-scale motors to be fired that are intentionally allowed to be pushed to limits, sometimes resulting in failure. This atmosphere fosters a positive research environment.

ABSTRACT

For the last several years, the Naval Air Warfare Center Weapons Division (NAWCWD) has participated in an extensive effort to understand nonlinear pulsed instability in tactical sized solid rocket motors. The purpose of this work was to broaden the knowledge of design factors that influence nonlinear axial mode combustion instability. This effort concentrated on reduced smoke propellant systems at pressures around 6.9 megapascals (Mpa). During this effort 23 pulsed motor firings were performed. A brief review of these firings will be presented in this paper.

Another new effort has also been undertaken over the last several years to examine pulsed instability in reduced smoke systems operating at higher pressure. In this paper, combustion instability data are presented on eight tactical size motor firings. The parameters investigated in these firings were the effects of pressure and pulse amplitude on nonlinear pulsed instability. Each motor was pulsed two to three times during burn. The motors were instrumented with two or three high-frequency piezoelectric quartz pressure transducers. The motors with three transducers had them mounted at the forward, middle, and aft ends of the motor. Acoustic data are presented and compared with linear stability predictions made by the Standard Performance Prediction/Standard Stability Program (SPP/SSP) computer code. Included in the paper are laboratory response testing results. As previous studies indicated, results indicate a significant adverse effect on nonlinear stability as pressure is increased. Second, the stability boundary was determined by bracketing the pulse amplitude required to trigger a motor into high levels of combustion instability. Third, placement of three transducers mounted along the length of the motor determined the hard-to-obtain waveform and phase data of a motor undergoing combustion instability. Finally, results showed that it is possible to pulse a motor into nonlinear limiting amplitude oscillations, even when the propellant contains a stability additive.

INTRODUCTION

The Naval Air Warfare Center Weapons Division (NAWCWD) at China Lake has participated in a program to develop an improved understanding of linear and nonlinear combustion instability in solid propellant rocket motors. One primary goal of this program was to develop a systematic database of motor and stability data for future analysis. Earlier papers have reported on previous NAWCWD work on this program (References 1 through 4). This past work will be briefly reviewed here.

The motors fired in the past program were 12.7 centimeters (cm) in diameter and 170 cm in length. The majority were loaded with an 88% solids reduced smoke AP/HTPB propellant with a nominal burning rate of 0.61 cm/sec at 6.9 megapascals (Mpa). In addition, motors were fired which contained 1% by weight 8-micron aluminum oxide, 90-micron aluminum oxide, and 3-micron zirconium carbide as stability additives in place of 1% ammonium perchlorate. Motor pressures ranged from 3.45 to

10.3 MPa. Pressure coupled combustion response measurements were made with a t-burner at the nominal motor operating pressures for all propellants.

Several motor configurations and propellant variations were included in the program. Twenty-three motors were fired and each motor was typically pulsed three times during burn. The baseline grain geometry was a six-point star in the aft two-thirds of the motor and a cylindrical section in the forward end. Most of these motors were fired using the baseline reduced smoke composite propellant and three were fired with propellants containing stability additives. Three motors with star forward grains, one motor with a full star grain, two motors with cylindrical cross sections, and four half-length higher frequency motors were fired. The pulsing produced 10 unstable pulses (pulses that grew to a limiting oscillatory amplitude) and 32 stable pulses (pulses that decayed). A complete description of the motors can be found in References 1 and 2. Table 1 summarizes the data produced by these motor firings, and Table 2 shows the differences among the propellants for these firings. Figure 1 contains a sample ballistic pressure trace of motor no. 4 from Table 1. In this figure, a stable pulse can be seen around 1 second and an unstable pulse around 2 seconds. Numerous conclusions were reached from these first 23 motor firings. They are summarized by subject below.

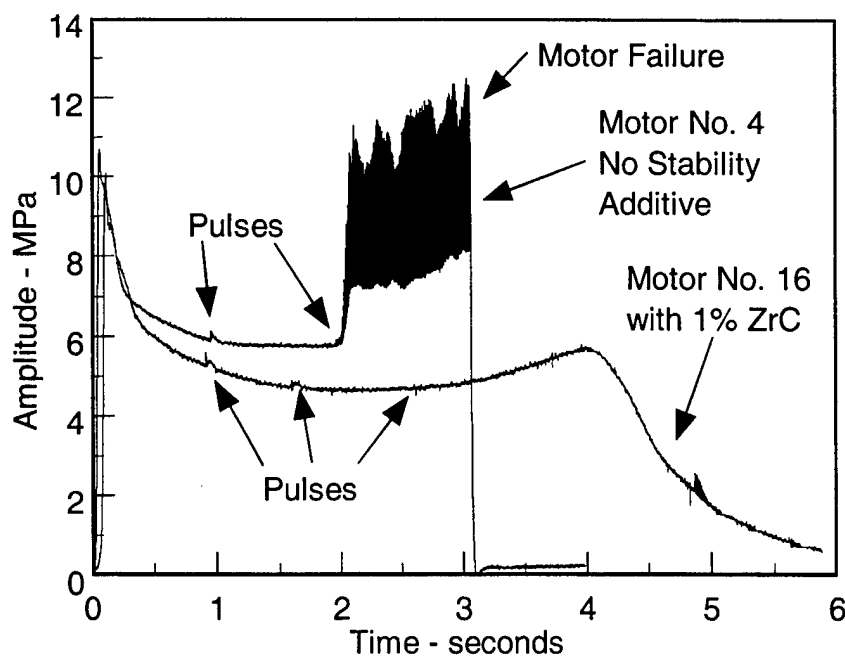


FIGURE 1. Comparison of Motor No. 4 Without Stability Additive and Motor No. 13 With 1% ZrC Stability Additive.

Pressure. As chamber pressure is increased, the margin of linear stability decreases. Higher pressure motors are more susceptible to pulsed instability at lower pulse amplitudes. The severity of the instability appears to be independent of mean chamber pressure.

TABLE 1. Motor Test Matrix for Past Program.

Test No.	Geometry	P _{avg} , MPa	NWR Prop No.	Pulse No. 1				Pulse No. 2				Pulse No. 3			
				Time, Sec	Web, cm	Pulse, kPa	α , 1/sec	Time, sec	Web, cm	Pulse, kPa	α , 1/sec	Time, sec	Web, cm	Pulse, kPa	α , 1/sec
1	SAFT3	5.52	11	nrd	--	--	--	2.016	1.270	248	+209	osc	--	--	--
2	"	"	"	0.703	0.503	83	-159	1.708	1.092	83	+207	osc	--	--	--
3	"	"	"	0.805	0.566	97	-112	1.790	1.240	345	+161	osc	--	--	--
4	SFWD3	6.21	"	0.970	0.864	262	-190	1.962	1.506	152	+56	osc	--	--	--
5	SAFT3	5.52	"	0.965	0.660	690	-176	npf	--	--	--	npf	--	--	--
6	"	3.72	"	0.760	0.467	124	-214	2.005	1.092	48	-102	3.010	1.549	41	-75
7	SFUL3	6.21	"	0.748	0.640	262	+639	osc	--	--	--	osc	--	--	--
8a	SAFT3	5.52	"	npf	--	--	--	npf	--	--	--	3.020	1.816	69	+134
8b	"	3.72	"	0.950	0.559	345	-210	2.216	1.181	138	-89	3.419	1.732	221	+366
8c	"	10.3	"	0.617	0.538	138	+151	osc	--	--	--	osc	--	--	--
8d	"	5.52	"	npf	--	--	--	npf	--	--	--	npf	--	--	--
9	CYL3	5.72	"	0.745	0.351	138	+232	osc	--	--	--	osc	--	--	--
10	"	4.21	"	0.887	0.406	248	+244	osc	--	--	--	osc	--	--	--
11	SAFT6	3.31	11b	2.067	0.815	276	-143	3.688	1.445	41	-75	5.218	2.507	28	-60
12	"	5.52	"	1.374	0.599	83	-182	2.543	1.102	41	-247a	nrd	--	--	--
13	CYL6	4.00	"	1.261	0.442	55	-185	2.429	0.902	28	nrd	3.445	1.334	28	-71
14	SFWD6	4.55	"	1.945	0.930	345	-201	3.465	1.631	55	-133	4.898	2.319	14	-33a
15	SAFT3	6.48	12	0.948	0.719	1200	-122	1.764	1.242	276	-84	nrd	--	--	--
16	"	4.96	13	0.824	0.533	359	-232	1.505	0.899	179	-137	nrd	--	--	--
17	"	5.72	17	0.866	0.579	483	-188	1.660	1.044	317	-75	2.572	1.542	14	-110a
19	SAFT3	10.1	11b	nrd	--	--	--	1.817	1.247	14	-26a	2.767	1.842	14	-64a
20	SFWD3	5.03	"	0.984	0.752	110	-193	2.167	1.402	28	-81	npf	--	--	--
21	"	"	"	1.012	0.770	290	-251	2.195	1.417	69	-143	3.506	2.060	28	nrd

NOTE: npf = no pulse fired; nrd = not reducible; osc = oscillating; a = weak pulse
Actual pulse amplitude determined by extrapolation back to zero time.

TABLE 2. Propellant Matrix for Past Program.

Propellant No.	Additive	Size, micron	Rate,* cm/sec	Response,** R_p	Exponent, n
NWR-11	(none)	---	0.605	1.25	0.491
NWR-11b	(none)	---	0.541	2.20	0.461
NWR-12	Al ₂ O ₃	3.5	0.630	0.75	0.493
NWR-13	ZrC	3.5	0.572	0.82	0.493
NWR-17	Al ₂ O ₃	90.0	0.584	0.79	0.413

* Burning rate at 6.9 Mpa.

** Response function at 6.9 MPa and 300 Hertz (Hz).

Stability Additives. Stability additives were very effective in preventing nonlinear pulsed combustion instability. However, differences between different stability additives were not evident. Figure 1 shows how effective additives can be. In this figure, both motors are identical except one has 1% ZrC and one does not. In fact, the one with stability additive was actually pulsed harder. Stability additives suppress instabilities by increasing particle damping and/or reducing the propellant response over a broad frequency range. Nonlinear instability tendencies are reduced in motors with additives.

Stability Calculations. Stability calculations compared very favorably with motor data, especially for one-dimensional (1-D), high length/diameter (L/D) motors without

metal combustion. An example of this is shown in Figure 2. It is also important to note that the margin of linear stability decreases with burning time.

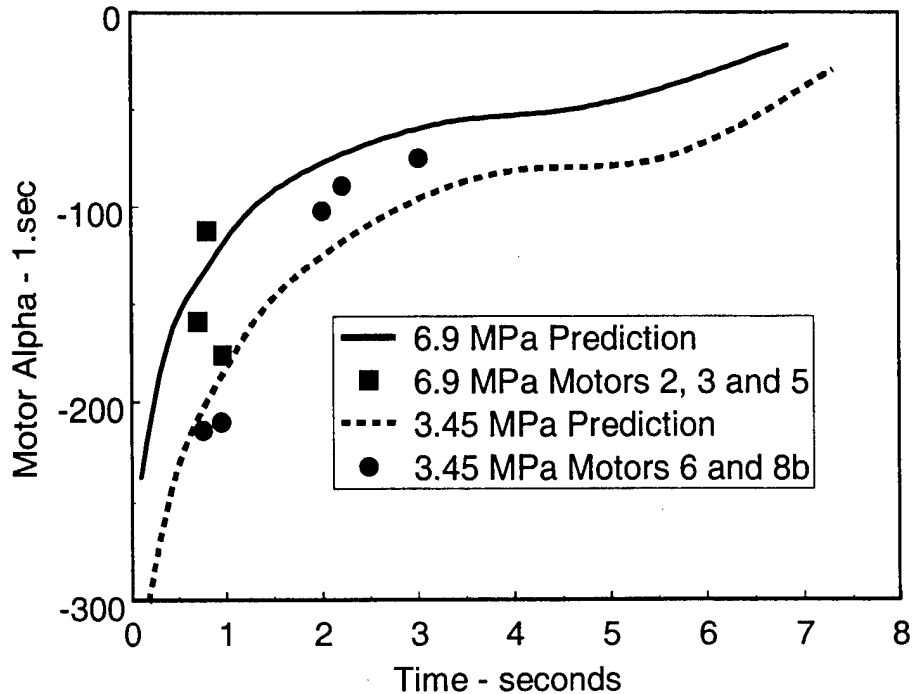


FIGURE 2. Measured and Predicted Star Aft 300-Hz Motor Alphas Comparison With Theoretical Predictions.

Geometry. Motor geometry comparisons were made that indicated that a star forward geometry was more stable than a star aft geometry. This conclusion was validated both experimentally and theoretically. This implies that an increase in burning surface area in the aft end reduces the margin of stability. In addition, the constant-cross section geometries (full star and full cylinder) were both observed to be very sensitive to pulsing and resulting instabilities.

Pulsing. Pulsing motors can give quantitative data, i.e. margin of stability. Routine pulsing of developmental motors is encouraged. High pulse amplitudes can excite instability in an otherwise stable motor. Pulsing a low-pressure motor is easier than pulsing a high-pressure motor, especially at low pulsing levels where the pulser burst pressures are similar to the motor chamber pressures.

Nonlinear Effects. Pulsing susceptibility of reduced smoke systems is related to linear, high-frequency combustion response characteristics. Both growth and decay alphas are independent of pulsing amplitude for linear but not nonlinear systems. The susceptibility to pulsed instability increases with decreasing gas mean flow velocity. Finally, the magnitude of the direct current (DC) pressure shift is linearly proportional to the limiting amplitude.

MOTOR FIRINGS DETAILS

In the design community, there has been a concerted effort to develop tactical solid rocket systems, which have greatly reduced plume signatures. The combustion instability of these systems is of particular concern because the metal oxide particles that provide acoustic damping are absent. Some of the suggested propellants for these systems have considerably less energy. One way to gain some of the performance lost is to increase the motor operating pressure. Fortunately, many modern rocket motors use composite cases that have excess capacity to support hoop stress and can handle the added pressure without a weight penalty. However, as indicated above, some of the data generated and analysis performed during the course of this program indicated a possible increase in instability tendencies at high motor operating pressures. This was also shown in past studies (References 5 through 10). The loss of particulate damping and the higher operating pressures may cause combustion instability to be a problem in future motors. Therefore we decided to fire and pulse additional motors, concentrating on pressure effects and stability additives. In addition, one area where the above data were lacking was in the determination of the actual pulsing level required to pulse a motor into nonlinear combustion instability. To examine this level, we decided to vary the pulse amplitude. The following pages describe motor firing results and analysis for varying pressure, stability additive, and pulsing levels for 10 motors fired from 1994 to 1997.

Propellants. Table 3 shows the two different formulations used during these motor firings. Unfortunately, these propellants differ in more than one way, making conclusions about formulation effects difficult. There is one important difference, however, from which conclusions can be drawn. Propellant A contains 1% of the proven stability additive, zirconium carbide (ZrC). In past motor firings it was difficult to pulse a motor containing a stability additive into instability. More on this will be discussed later in the paper.

Test Matrix. Table 4 shows the testing matrix for the ten motor firings. All motors fired in the program were 12.7 cm in diameter and 170 cm in length. In addition, all motors were typically pulsed two to three times during burn. Motors no. 1 and 2 both failed during firing. Motors no. 3 through 5 were identical except for the nozzle throat size, which caused the chamber pressure to vary. These three used the reduced smoke propellant without additive, propellant "B," and were full cylinder geometries. The purpose of these motors was to look at the effect of pressure on nonlinear pulsed instability. All three motors were pulsed with similar pulsing levels, three times during burn. Motors no. 6 through 9 were star aft motors loaded with propellant "A" given in Table 3. Motor no. 10 was a full cylinder motor containing propellant "B." The purpose of Motors no. 6 through 9 were to see what effect pulsing amplitude would have on the stability of the motors. Motors no. 6 and 7 were pulsed at 5 and 3% levels at 33 and 66% of the web burned. Motors no. 8 and 9 were pulsed at 10 and 6% levels. A pulse of 3% means that the desired pulse amplitude was to be 3% of the current chamber pressure in the motor. Because of uncertainties in pulsing motors, the exact desired amplitudes were not always obtained; this will be discussed later. To look at effects of increasing motor pressure, motors no. 6 and 7, with the light pulses, were fired at mean chamber pressures of 6.9 and 10.3 MPa, respectively. Likewise, motors no. 8 and 9, with the hard pulses, had chamber pressures of 6.9 and 10.3 Mpa, respectively, as well. The intent of motor

no. 10 was to repeat the second firing of the previous year's motor firing, motor no. 4, but with added instrumentation (Reference 3).

TABLE 3. Propellants.

Propellant	"A" Reduced smoke with additive	"B" Reduced smoke no additive
Ingredient	Approximate weight %	Approximate weight %
AP	82.0	86.5
RDX	4.0	--
HTPB	12.5	13.0
Carbon black	0.5	0.5
ZrC	1.0	--
Burning rate @ 6.9 MPa	0.678 cm/sec	0.879 cm/sec
Exponent @ 6.9 MPa	0.360	0.392
Response @ 6.9 MPa	1.55	1.80
Propellant density	1.80 g/cm ³	1.72 g/cm ³
Flame temperature @ 6.9 MPa	2713°C	2748°C
Speed of sound @ 6.9 MPa	1083 m/sec	1077 m/sec

TABLE 4. Motor Test Matrix.

Motor no.	Firing date	Pressure, MPa	Propellant	Geometry	Case hardware	Comments
1	1994	20.7	RS with additive	Star aft	Light	Motor failed
2	1995	20.7	RS with additive	Star aft	Light	Motor failed
3	1996	3.45	RS	Full cylinder	Heavy	Pressure effects
4		10.3	RS	Full cylinder	Heavy	
5		13.8	RS	Full cylinder	Heavy	
6	1997	6.90	RS with additive	Star aft	Light	Enhanced instrumentation, stability additives, pulsing magnitudes and geometry effects
7		10.3	RS with additive	Star aft	Light	
8		6.90	RS with additive	Star aft	Light	
9		10.3	RS with additive	Star aft	Light	
10		10.3	RS	Full cylinder	Heavy	

RS = Reduced smoke propellant.

Pulsers. The standard NAWCWD pulsers were used on the firings (References 1 through 4). By using the results of subscale testing and past motor firings, the pulsers were sized to give the desired pulse amplitude. The subscale results were scaled by knowing the motor volume and pressure and choosing a laboratory pulser baseline that was closest to the test conditions. The pulser was then fine tuned by adjusting the charge amount to motor pressure, gas density, and volume conditions (Reference 2). A schematic of the pulser is shown in Figure 3. The pulser pressure gauges were used on some of the early motor firings and during pulser subscale testing. The final pulser parameters used during these tests are shown in Table 5.

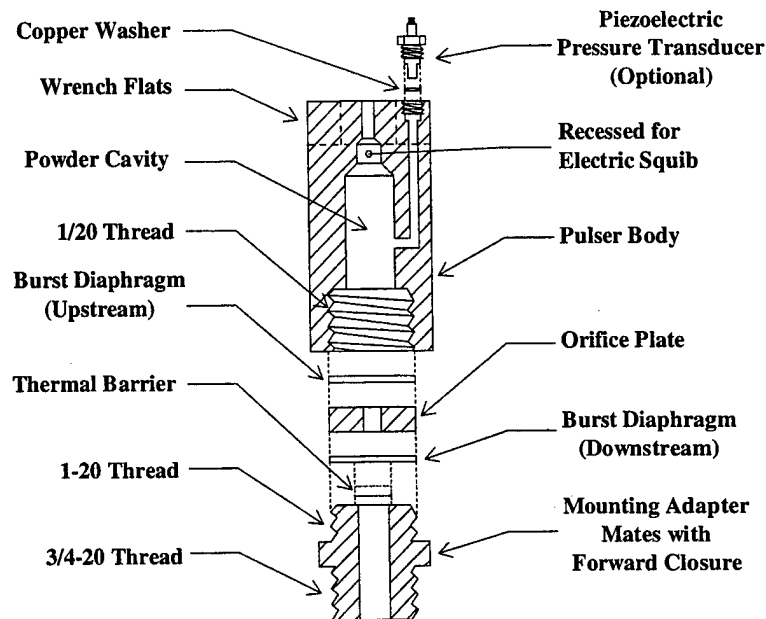


FIGURE 3. Pulser Schematic.

Instrumentation. Each motor was instrumented with either two or three water cooled Kistler 211B2 piezoelectric quartz gauge and one low frequency strain gauge type pressure transducer. Also mounted on the motor were two or three pulsers and the igniter. All data were recorded at 20,000 samples per second with a 16-bit analog-to-digital converter with a 10,000-Hz anti-aliasing filter, recorded on frequency modulated (FM) Wide Band I tape with one channel per tape track at 60 inches per second (ips), and recorded on multiplexed FM tape. The digital sample rate per channel was limited by the analog to digital conversion system, by the number of signals recorded, and the duration of the test. Each high-frequency gauge was split three ways: (1) DC coupled data scaled to the maximum expected pressure of the test; (2) low gain alternating current (AC) coupled data high pass filtered at 80 Hz with a typical gain of two; and (3) high gain AC coupled data high pass filtered at 80 Hz with a typical gain of 10. The high gain signal provided good resolution of low level AC signals up to several hundred pounds per square inch (psi), the low gain gave good resolution of higher level AC signals up to 5,000 psi, and the DC data provided a comprehensive view of the data from zero to 10,000 psi. It is important to note that the DC pressures obtained by the Kistler gauges

are not very accurate due to a slight drifting of the signal with time. The AC component is very accurate. The strain gauge pressure transducer was used for accurate ballistic pressure. The Kistler amplifiers were usually set at sensitivities of either 3.45 or 6.9 MPa per volt depending upon the expected pressure in the motor. Standard S-Video and 1,600 frames per second movies were also taken of each firing at various angles. In addition, flash bulbs went off on the motor test stand coinciding with each pulse and ignition. In the figures that follow, the digital data were used and the data channel providing the highest resolution of the signal of interest was used. All transducers and data channels worked successfully, although some of the high gain channels did saturate during oscillations. Signal saturation was expected and is the reason low gain channels were also recorded.

TABLE 5. Pulser Details.

Motor no.	Pulse no.	Time, sec	Orifice, mm	Upstream diaphragm, mm	Downstream diaphragm, mm	Charge amount, g	Est. pulser amp, kPa	Est. pulser amp % mean P	Est. motor pressure, MPa
1	--	--	--	--	--	--	--	--	--
2	--	--	--	--	--	--	--	--	--
3	1	1.12	3.66	5.08	5.08	0.2	138	5.0	2.76
	2	2.15	5.05	--	5.08	0.1	93	3.0	3.10
	3	3.13	7.49	--	5.08	0.1	34	1.0	3.45
4	1	0.97	2.51	5.08	5.08	0.1	345	5.0	6.90
	2	1.92	7.49	--	5.08	0.1	259	3.0	8.62
	3	2.90	2.51	--	0.05	0.1	103	1.0	10.3
5	1	0.50	2.51	5.08	5.08	0.11	448	5.0	8.96
	2	1.00	7.49	--	5.08	0.11	310	3.0	10.3
	3	1.50	2.51	--	1.27	0.14	138	1.0	13.8
6	1	1.00	3.66	2.54	2.54	0.1	355	5.0	7.10
	2	2.00	3.66	2.54	2.54	0.1	197	3.0	6.55
7	1	0.865	3.66	2.54	2.54	0.1	535	5.0	10.7
	2	1.715	3.66	2.54	2.54	0.1	306	3.0	10.2
8	1	1.00	2.51	5.08	5.08	0.2	710	10.0	7.10
	2	2.00	2.51	5.08	5.08	0.2	393	6.0	6.55
9	1	0.865	2.51	5.08	5.08	0.2	1069	10.0	10.7
	2	1.715	2.51	5.08	5.08	0.2	612	6.0	10.2
10	1	0.97	2.51	5.08	5.08	0.1	345	5.0	6.90
	2	1.92	7.49	--	5.08	0.1	259	3.0	8.62

Motors no. 1 through 8 had two high-frequency Kistler gauges mounted in the forward closure. This was identical to past motor firings (References 1 through 3). For motors no. 9 and 10, three identical Kistler gauges were mounted along the length of the motor. The first was located at the forward closure, like motors no. 1 through 8. The second was located at the middle of the motor, and the third was located very near the nozzle entrance at the aft end. The middle and aft gauges were installed by drilling a hole through the 4-cm case wall and on through the propellant. The propellant was then inhibited to prevent burning on the inside of the hole. The purpose of these gauges was to examine wave structure and phase relationships of the acoustic oscillations in the motor.

Motor Failures. The first two motors fired in the test program ended in failure. Motor no. 1 failed 35 milliseconds into the motor firing, when the aft closure snap ring failed and the forward closure containing all of the instrumentation was injected, destroying all instrumentation and the pulsers, and ruining the motor firing. The instrumentation worked long enough to show that the motor did reach 28 MPa when the failure occurred, and the two Kistler gauges recorded the drop in pressure as the closure flew off the motor. High-speed photography at 1,000 frames per second showed the failure. Because the failure occurred so early in burn, the pulser performance could not be verified.

Motor no. 2 was fired in the summer of 1995. Unfortunately, the pressure exceeded 48 MPa and explosively blew off the forward closure, all retaining hardware, and all pulsers and instrumentation. The structural failure of motor no. 1 was caused by a faulty snap ring installation as described above; however, the poor installation may have only allowed the motor to fail at a lower pressure. The motor no. 2 firing had significant reinforcing hardware added to hold the closures on. It is now believed that the added hardware only delayed the failure and made more it severe.

Propellant "A" was initially believed to have a constant exponent up to 28 MPa. Unfortunately, it was later discovered that the burning rate curve data at higher pressures was merely extrapolated data from low pressures. With the constant exponent curve, the motor was predicted to have a peak pressure of 29 MPa immediately after ignition and then return to a mean value of 21 MPa for the remainder of the firing. This pressure profile is now believed to take the propellant ballistics into a higher exponent region of the burning rate curve, and the ballistic calculations now show that the motor could easily reach 41 MPa or greater. These two failures forced a lowering of the chamber pressures for future firings and a complete redesign of the motor hardware. This is why the "heavy walled" cases described below were fabricated. In addition, to minimize the ignition-erosive burning spike at the beginning of burn, the geometry was changed to a full cylinder configuration.

Motor Hardware. Reliable motor hardware is essential for successful firing and pulsing of motors, especially at higher operating pressures. Two types of motor cases and end closures were used, although the internal geometries of both types were identical. The difference between the cases was the wall thickness and fastening method of the forward and aft closures. Although both types are very heavy duty and reusable, one is extremely heavy duty. For the purposes of this paper, the really heavy cases, which were 20 cm in diameter with screw-on end caps to hold the nozzle and forward closure assemblies, were called "heavy weight cases" (see Table 4). The smaller, 17.8-cm diameter cases with snap ring closures at both ends were called "lightweight cases." The snap rings proved to be unreliable at the high motor chamber pressures, as indicated above. In the heavy weight motors, the threaded end cap design allowed for much greater strength and reusability over the previous snap ring installation of the forward and aft closures. Table 4 indicates what type of case was used with each motor fired. Both cases had an inside diameter of 12.7 cm with an inside length of 170 cm. Both were made of stainless steel. In addition, the heavy walled cases were heat-treated. The heavy cases are good to 70 MPa while the light cases are good to 35 MPa. Both sets of hardware were completely reusable except for the nozzle. Each assembled motor

weighed more than 230 kilograms (kg) and the cast propellant weight was approximately 23 kg. The forward closure, which held the instrumentation, pulsers, steady state pressure gauge, and igniter, and the aft nozzle assemblies were compatible with both motor designs. Figure 4 shows the internal geometry for the star aft motor and a schematic of the instrumentation typically used for each firing. The pulser pressure gauges were only used on some of the firings.

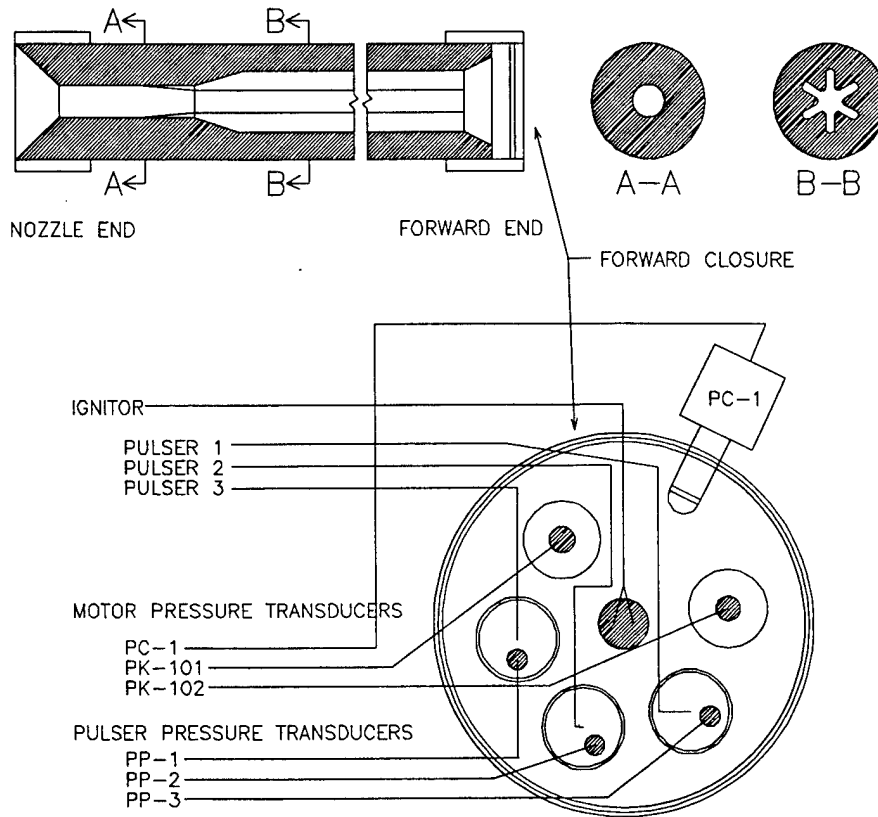


FIGURE 4. Motor Geometry and Forward Closure Instrumentation.

FIRING RESULTS AND ANALYSIS OF MOTORS NO. 3 THROUGH 5

Motors no. 3 through 5 were fired in the summer of 1996. The principal intent of these motor firings was to examine the effect of increasing motor pressure on pulsed nonlinear combustion instability. Figure 5 shows the ballistic pressure traces of the three motors with the ballistic prediction (dashed line) for each motor. The predicted pressures followed the experimental traces fairly well until the onset of instability. The instability results of each motor firing are described below.

Motor No. 3. Motor no. 3 was a low pressure 3.45-MPa motor that was pulsed three times as approximately 25, 50, and 75% of the web burned or at 1, 2, and 3 seconds. Each of the pulses decayed rapidly and no oscillations were sustained in the motor after the pulses. Movies and video taken of the motor firing showed flashes in the plume during each pulse. Also, there were two additional unplanned pulses due to debris

passing out through the nozzle. The pulse amplitudes and decay rates were measured and will be presented along with the other motor data later in this paper.

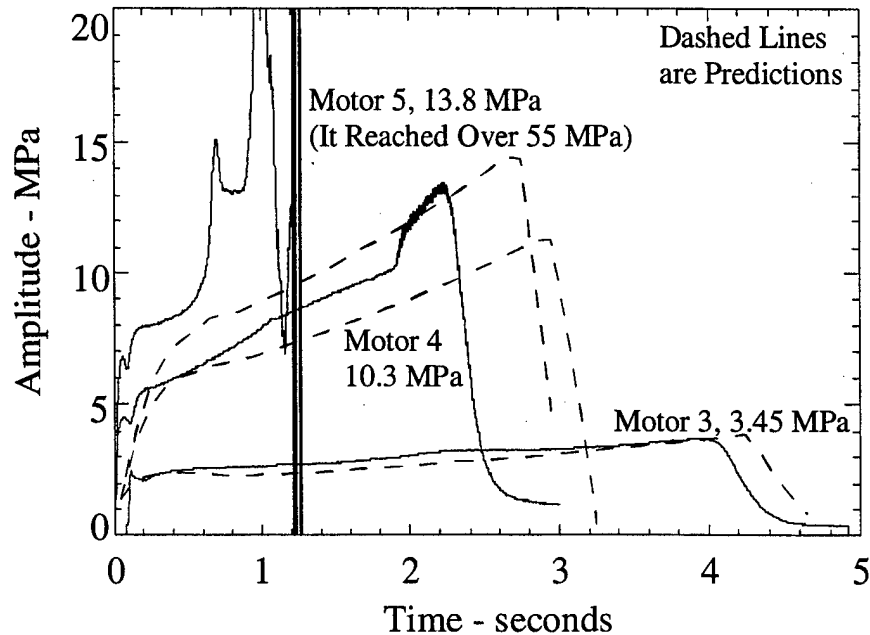


FIGURE 5. Ballistic Pressure of Motors No. 3, 4, and 5 Compared to Predicted Pressure.

Motor No. 4. Motor no. 4 was a higher pressure motor whose pressure ranged from 5.5 to 11.7 MPa during a normal burn. It was pulsed twice, at 1 and 2 seconds, corresponding to 40 and 80% of the web burned. The pulse timing was incorrectly set so the third pulse was after burnout. Motor oscillations decayed after the first pulse and grew after the second pulse. Figure 6 shows the DC coupled high-frequency data of the firing. There are several interesting items shown in this figure. The first pulse, which decays, can be seen at around 1 second. Immediately after the decay, some tangential oscillations are observed. The motor is reasonably quiet until the second pulse, which triggers the motor into violent nonlinear combustion instability.

Figure 7 shows the first pulse whose nonlinear peaks match the first longitudinal mode of the motor, which is 320 Hz. There is a very interesting observation concerning the high-frequency content of the pulse. Besides showing the nonlinearities of the pulse, it also corresponds to the first tangential mode of the case near the forward closure. These oscillations are observed in the traces of all pulses, both decaying and growing. Similar acoustic content was noted by Harris and others in recent work (Reference 10). At the forward end of the motor, the propellant stops 2.5 cm short of the closure containing the instrumentation and pulsers. The propellant face is inhibited. In this region of exposed case wall, the computed tangential mode is around 5,000 Hz. The first tangential mode is computed by:

$$\text{Frequency} = \frac{0.586 * (\text{Gas Speed of Sound})}{\text{Diameter of Chamber}} \quad (1)$$

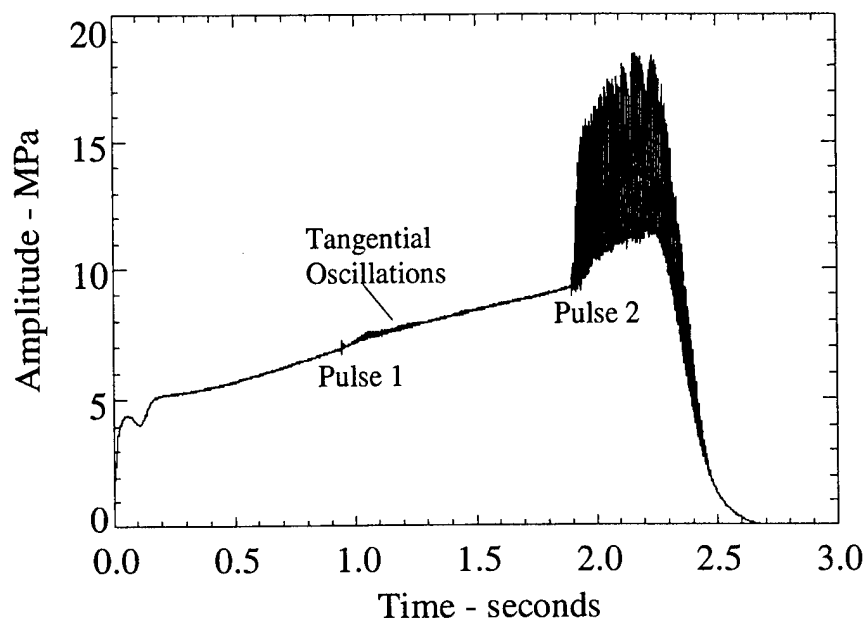


FIGURE 6. DC Coupled High-Frequency Ballistic Pressure Trace of Motor No. 4.

As mentioned above, after pulse one decays, spontaneous oscillations are observed. Figure 8 shows some details of these oscillations. Frequency analysis of the oscillations, seen in Figure 9, strongly suggests that these oscillations are the first tangential mode occurring around the inside of the cylindrical propellant surface. The labels on the vertical axis represent time slices, while the height of the peaks represent the amplitude of the oscillations at a given frequency. In the waterfall plot, the initial pulse can be seen containing many modes from the first longitudinal harmonic up to 7000 Hz. The pure tangential oscillations are seen next. Unlike the tangential oscillations noted above, whose frequency is constant, these show the traditional decreasing frequency shift as the oscillation progresses, from 6,700 to 6,400 Hz. The computed variation in frequency between 0.9 and 1.3 seconds in burn is from 6,847 to 6,357 Hz using Equation 1 and the properties from Table 3.

The second pulse is shown in Figures 10 and 11. An initial disturbance grows from an initial pulse of around 345 to 6,900 kPa in less than 10 cycles. In these two figures the DC component of the signal has been taken out by digitally high passing the data above 80 Hz. This serves two purposes. First, the DC pressure level is changing very rapidly, making determination about the AC component difficult. Second, it eliminates some minor 60 Hz signal noise that can distort the true data. A frequency analysis of the violent limiting amplitude oscillations of Figure 11 is shown in Figure 12. The first mode of 330 Hz is the most dominant and 20 more harmonic modes are present. Notice the larger tangential mode peaks at around 5,000 Hz due to longitudinal mode coupling with tangential oscillations around the front closure, as described above.

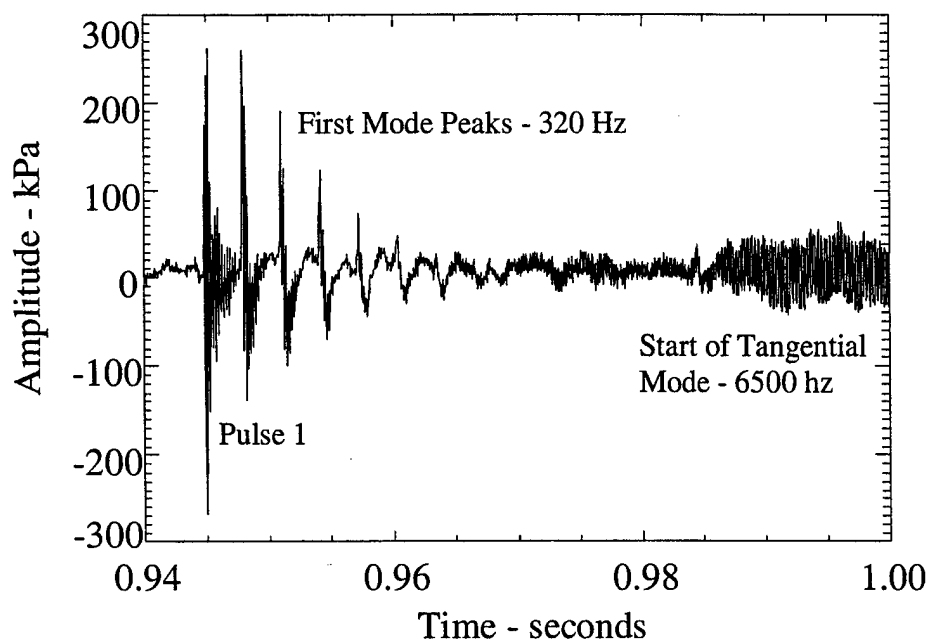


FIGURE 7. Details of Pulse 1 of Motor No. 4.

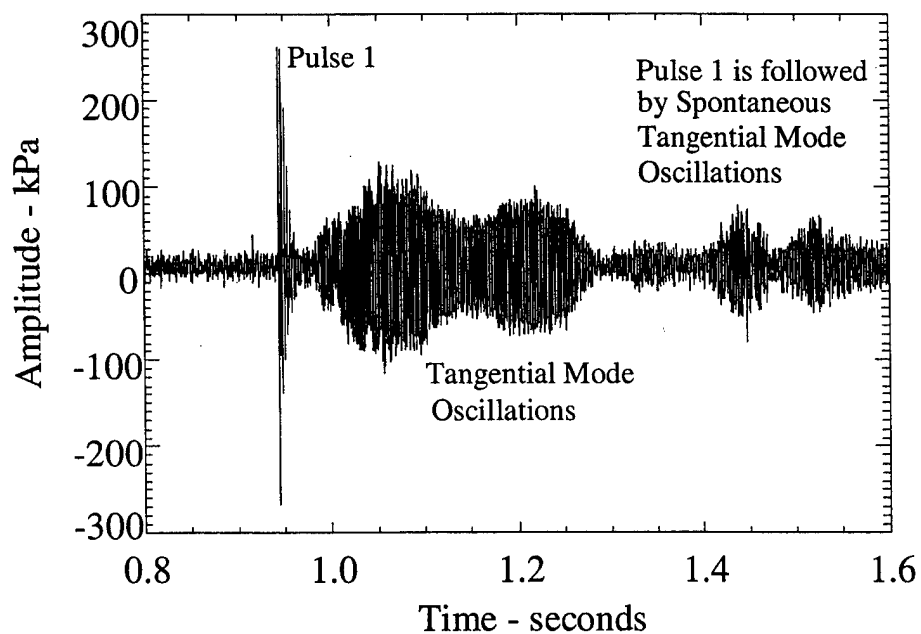


FIGURE 8. Details of Spontaneous Oscillations After Pulse 1 of Motor No. 4.

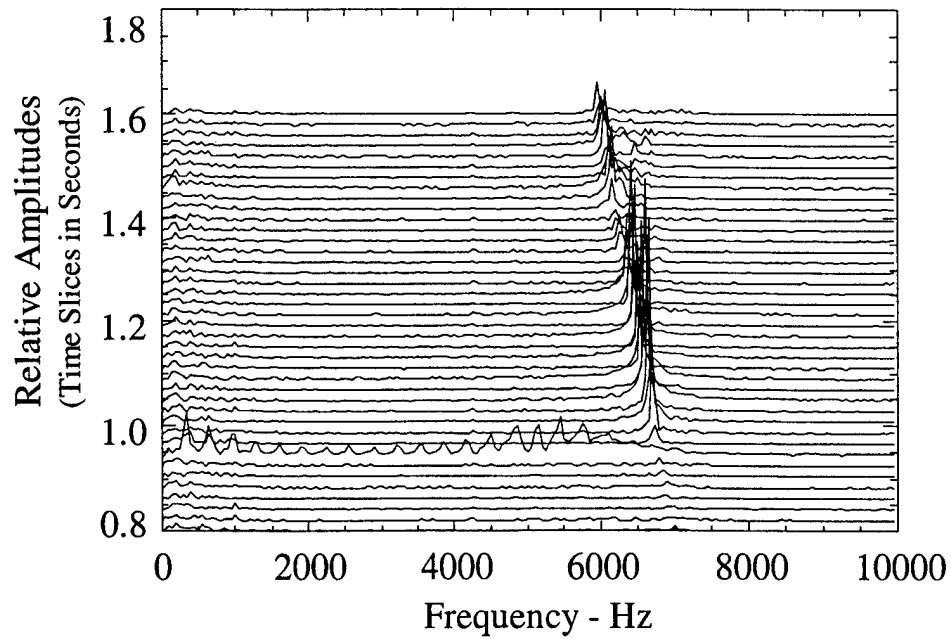


FIGURE 9. Frequency Analysis of Pulse 1 and Following Tangential Oscillations for Motor No. 4.

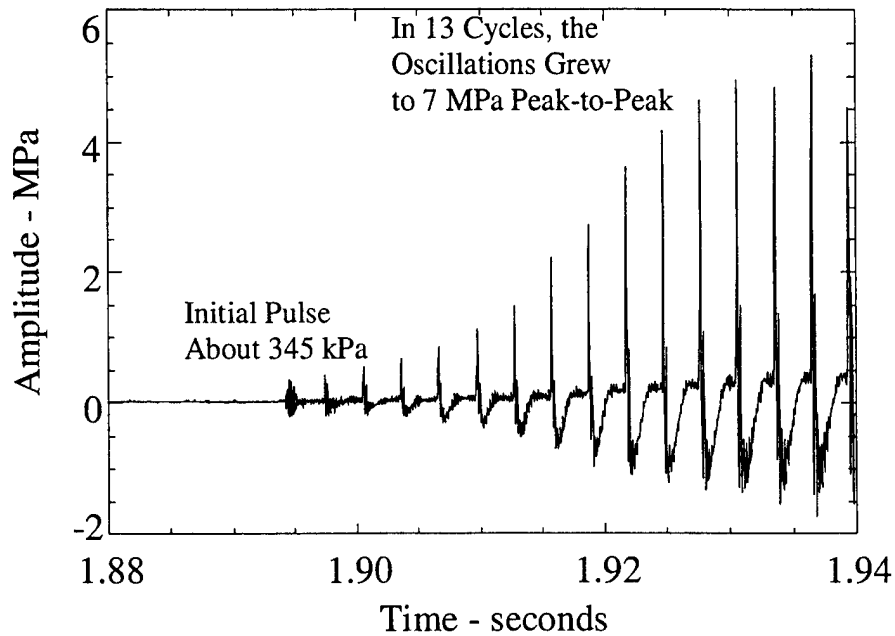


FIGURE 10. Details of Pulse 2 of Motor No. 4.

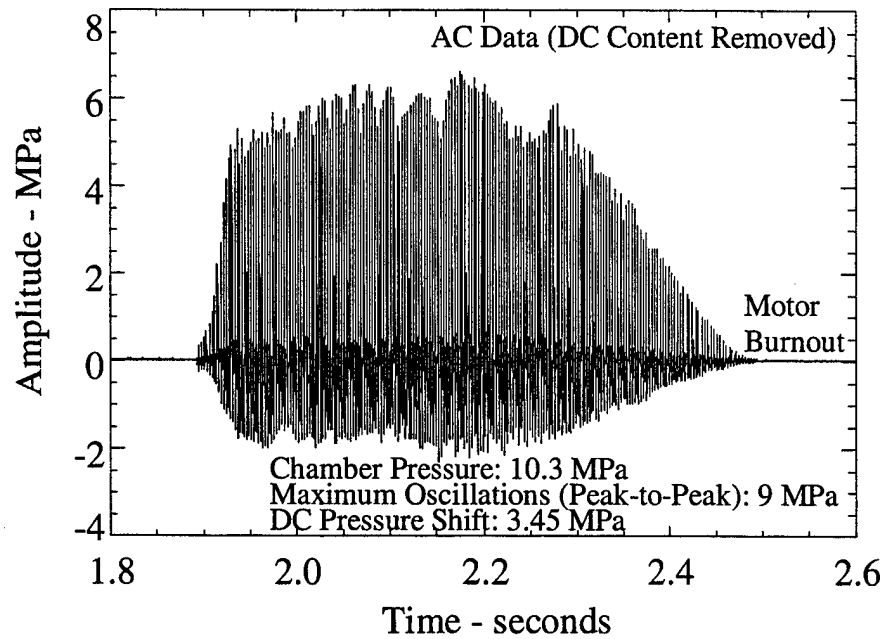


FIGURE 11. Limiting Amplitude Oscillations of Pulse 2 of Motor No. 4.

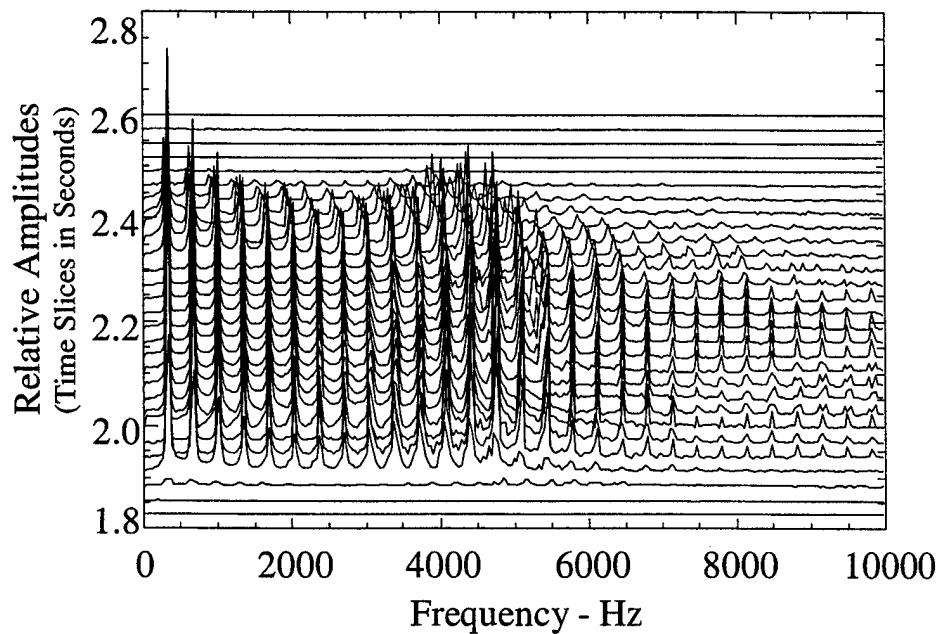


FIGURE 12. Frequency Analysis of Limiting Amplitude Oscillations of Pulse 2 of Motor No. 4.

Motor No. 5. Motor no. 5 was the highest pressure motor with pressure ranging from 8.3 to 13.8 MPa during a normal burn. Although the motor was scheduled to be pulsed three times, spontaneous tangential oscillations prevented the analysis or detection of any of the pulses. The motor went spontaneously unstable at around 0.5 second and, after some acoustic gyrations, failed at just over a second of the planned 2-second burn. Figure 13 documents the probable series of events that led to failure. The oscillations quickly increased to 6.9 MPa peak-to-peak with a 13.8-MPa DC pressure shift. At this point, it is believed that the nozzle partially failed. The resultant nozzle assembly bounced around in the motor until it blocked the nozzle at about 0.95 second. The pressure then increased dramatically to 55 MPa. At this pressure the nozzle blockage was ejected along with the nozzle assembly, and the instantaneous large aft end opening with 55-MPa chamber pressure caused the mean thrust of the motor to increase ten-fold to around 400 kilonewton (kN). A second possible scenario causing the massive over-pressurization deals with the fluid dynamics of the violent tangential mode oscillations. It is possible that these oscillations caused a “tornado” to form down the axis of the motor. This fluid dynamic vortex prevented the mean flow from escaping the motor through the nozzle due to a reduction of the effective nozzle diameter. The mean chamber pressure increased until the nozzle assembly was ejected from the motor. Like the previous scenario, the instantaneous large nozzle opening with 55-MPa chamber pressure increased the mean thrust of the motor to around 400 kN. Whatever the reason, the acoustic oscillations exceeded 21 MPa peak-to-peak and mean chamber pressure exceeded 55 MPa. The excessive thrust and violent oscillatory behavior sheared the four 16-mm grade-five bolts holding the motor to the test stand. The motor left the test stand and traveled about 150-meters up over a 15-meter-high earthen berm and into the surrounding desert. Amazingly, no damage was done to the test stand and the motor hardware except to the forward closure and instrumentation. The motor case and end caps were scratched but undamaged. Figure 14 is the AC component of the oscillations and shows the onset of oscillations. Again, the first tangential mode was the culprit. Figure 15 shows the frequency analysis of the oscillations. The downward trend in frequency from 7,000 to 6,600 Hz at approximately 1 second is followed by an actual increase in frequency. This occurs when the motor pressure increases dramatically, resulting in increased chamber temperatures and an upward frequency shift. The peaks at 1.1 seconds are due to the movement of the motor as it launched.

Linear Stability. One thrust of the overall program was to develop an improved understanding of nonlinear (pulsed) combustion instability. Linear stability aspects were studied on this program because the nonlinear (pulsed) instability of a motor is believed to be related to its linear stability. The linear stability of a motor is characterized by its exponential decay (stability) or growth (instability) of pressure oscillations as follows:

$$\hat{P} = P_0 e^{\alpha t} \quad (2)$$

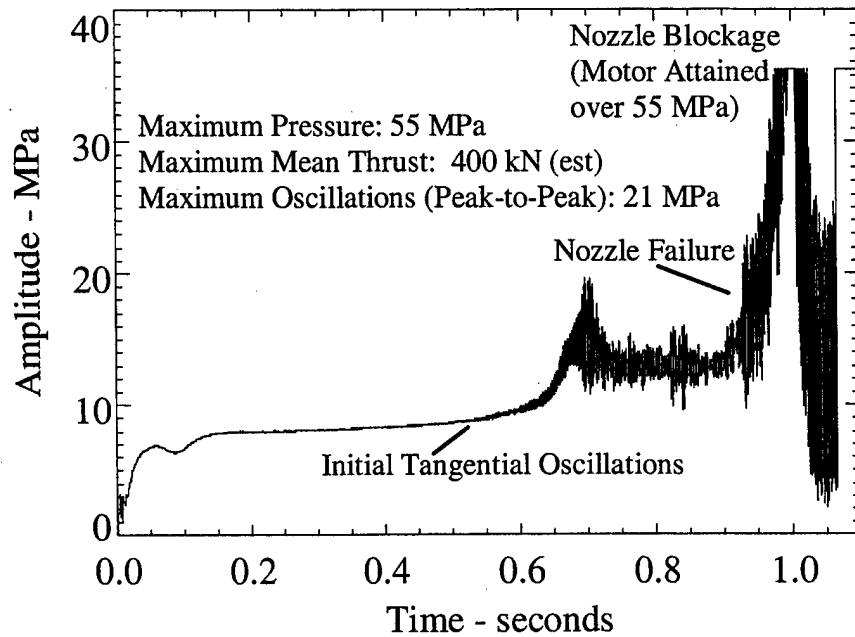


FIGURE 13. DC Coupled Ballistic Pressure of Motor No. 5.

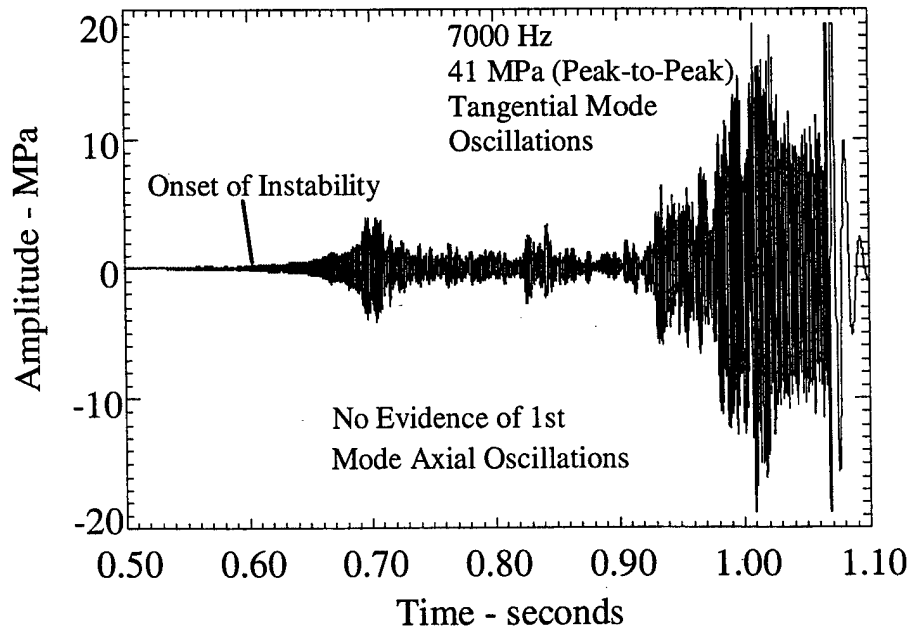


FIGURE 14. Details of Initial Oscillations That Led to Motor No. 5 Failure.

The rate of growth (or decay) is expressed in terms of the alpha in this equation. If a pressure perturbation in the motor is damped, the alpha is negative and the motor is linearly stable. If the perturbation excites a growth of pressure oscillations, the alpha is

positive and the motor is linearly unstable. Nonlinear instability, on the other hand, deals with the response to large or finite-amplitude (nonlinear) types of disturbances (References 5 through 10). Since knowledge of the linear stability was required, this facet of the program presented an opportunity to predict the linear stability of several motors and to make comparisons with linear experimental data that might be obtained under some test conditions. The Solid Propellant Performance computer program (SPP) and the one-dimensional Standard Stability Prediction computer program (SSP) were used to predict the motor performance and linear stability of the motors (References 11 and 12). The code's inputs include motor geometry, propellant ballistics, and the response of the propellant. The ballistic predictions shown in Figure 5 were performed using the SPP code. Figure 16 shows the pressure coupled response of the two propellants given in Table 3 at 6.9 MPa as measured by the t-burner (References 13 and 14). Response measurements were also made at other pressures corresponding to motor conditions.

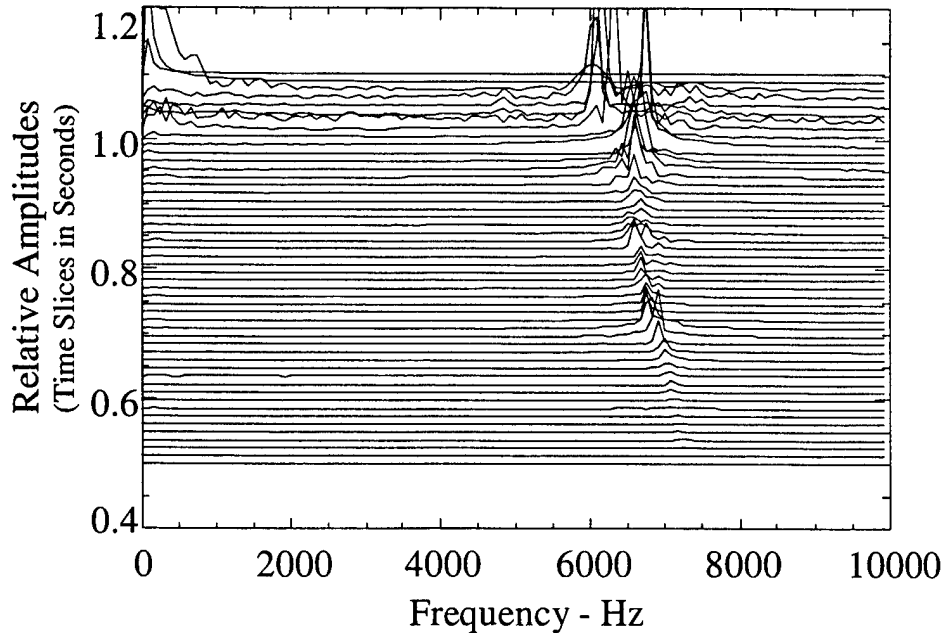


FIGURE 15. Frequency Analysis of Spontaneous Tangential Mode Oscillations of Motor No. 5.

Figure 17 is a 150- to 450-Hz digitally-band-passed-filtered trace of pulse 1 of motor no. 4 (see Figure 7). This signal is used to measure the linear decay of the fundamental first longitudinal mode produced by the pulse. The top graph in Figure 18 plots the absolute value of the filtered peaks of Figure 17 on a log scale versus time. The slope of this line is the decay alpha, α in Equation 2, and can be directly compared to the stability predictions. The bottom part shows the frequency of the decay, 330 Hz. Table 6 contains various parameters measured for motor firings no. 3-5. In it are the pulsing details, measured values of the decay alphas (like from Figure 17), linear growth alphas, DC pressure shifts, and limiting oscillatory amplitudes. Figure 19 compares the predicted

motor stability computed by the SPP/SSP program with the measured experimental data given in Table 6. The comparison is surprisingly good. The magnitudes of the total stability alphas produced by SPP/SSP and the trend of the data both agree with the predicted values. This type of comparison is similar to that seen in past studies (Reference 1).

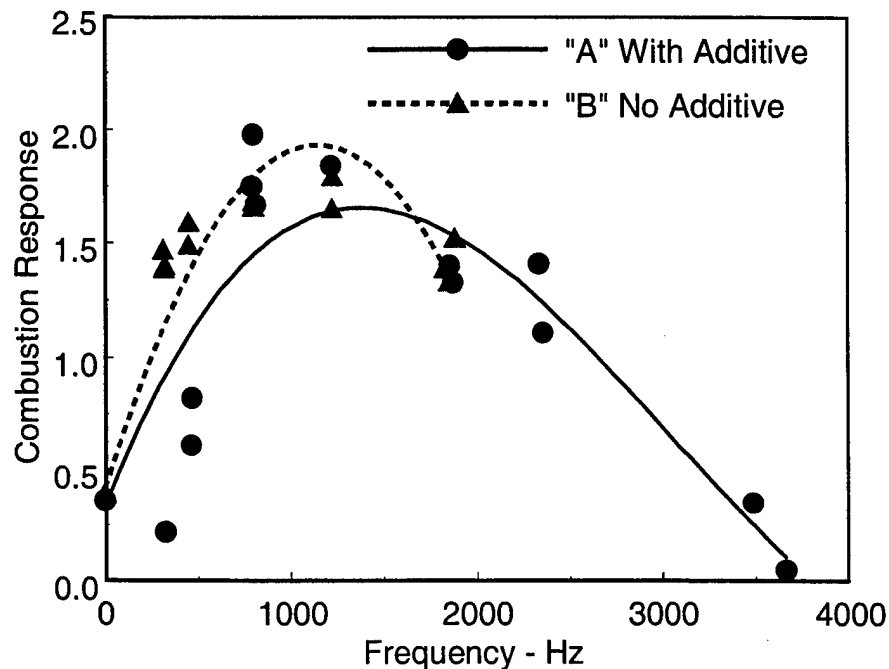


FIGURE 16. Combustion Response for "A" and "B" Propellants at 6.9 Mpa.

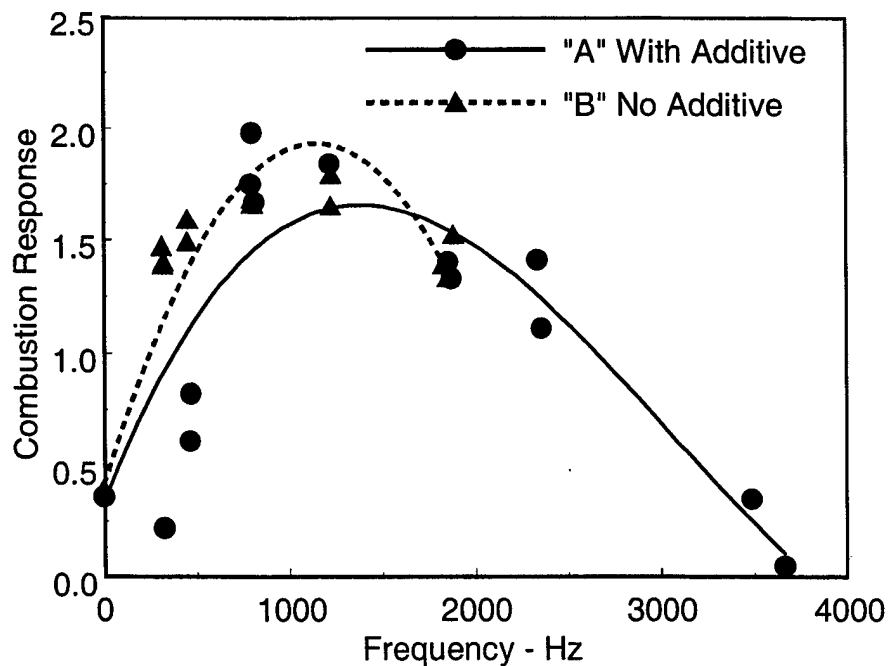


FIGURE 17. 150- 450-Hz Bandpassed Trace of Pulse 1 of Motor No. 4.

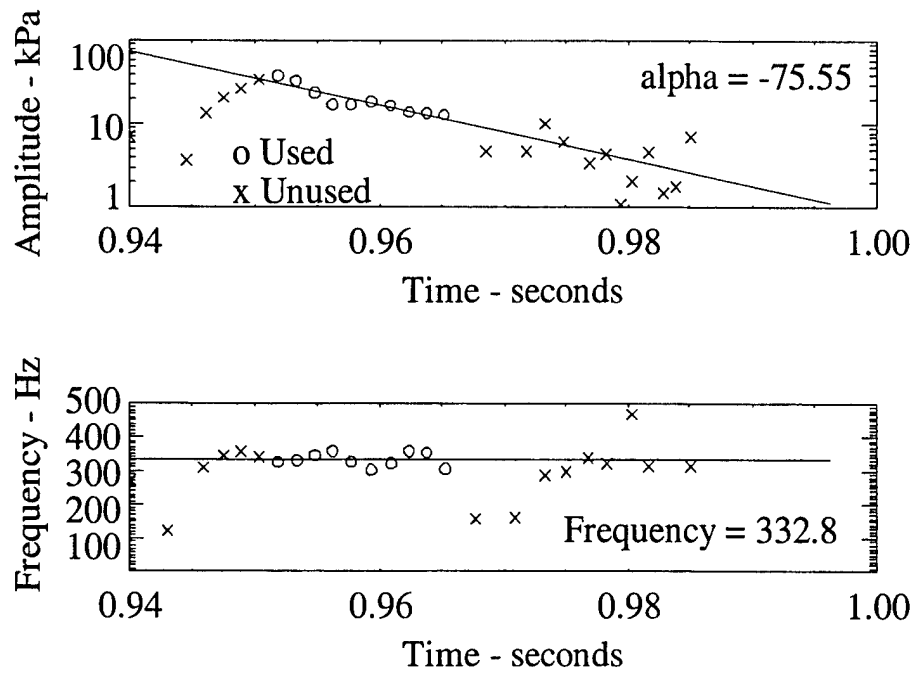


FIGURE 18. Decay Alpha and Frequency Determination of Pulse 1 of Motor No. 4.

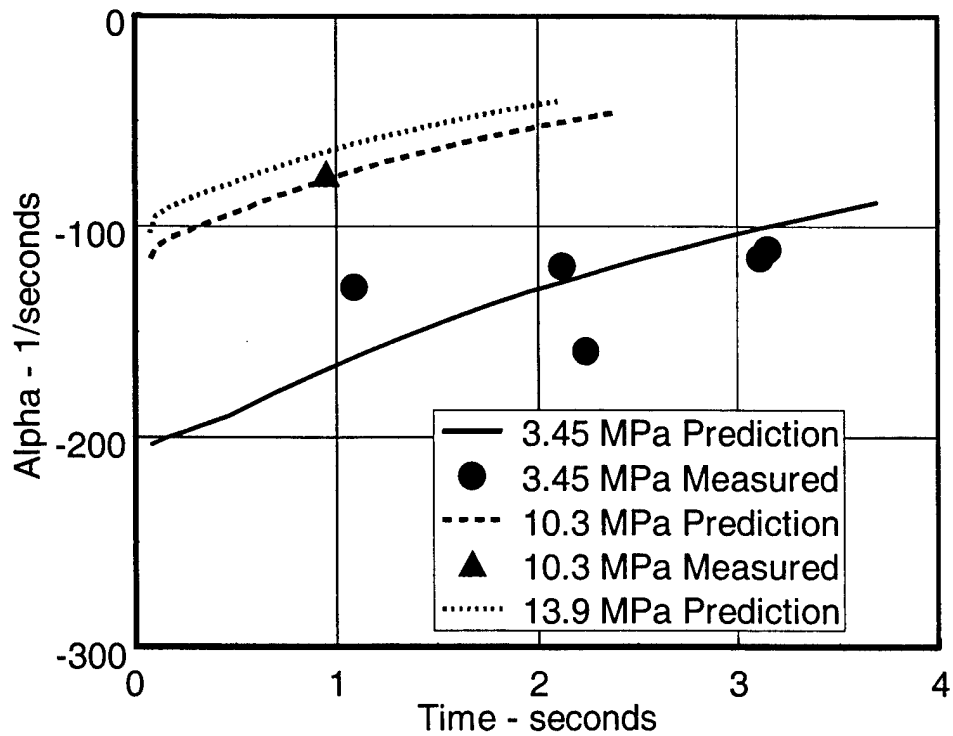


FIGURE 19. Stability Comparison of Stable Pulses for Motors No. 3, 4, and 5.

TABLE 6. Summary of Pulse Data for Motors No. 3 Through 5.

Motor no.	Pulse no.	Parameter							
		Chamber pressure, MPa	Est pulse, kPa	Pulse amp, kPa	Normalized pulse, % planned	Time, sec	Measured alpha, 1/sec	DC pressure shift, MPa	Limiting amplitude, MPa
3	1	2.6	138	345	13.3 (5.0)	1.09	-129	---	---
	2	3.2	93	172	5.4 (3.0)	2.12	-119	---	---
	2a (Injecta)	3.2	---	62	1.9	2.24	-159	---	---
	3	3.4	34	159	4.7 (1.0)	3.11	-115	---	---
	3a (Injecta)	3.4	---	28	0.8	3.15	-111	---	---
4	1	7.6	345	345	4.5 (5.0)	0.95	-75	---	---
	2	10.0	259	345	3.5 (3.0)	1.89	+109	3.45	9.0
5	Spontaneous	9.0	---	---	---	0.50	+21	6.9	9.0

There is an interesting observation worth noting about the growth rates, both of the first mode longitudinal oscillations in motor no. 4 and in the spontaneous first mode tangential oscillations of motor no. 5. The growth rate of both is linear. Figures 20 and 21 show this very nicely. Figure 20 is a plot of the growth rate amplitudes, band-pass filtered between 150 and 450 Hz. The linear growth rate is 109 1/sec. Figure 21 shows the same for the tangential oscillations except band-pass filtered between 3,000 and 9,000 Hz. Again the growth rate is linear and has a value of 22 1/sec. These data should be of interest to combustion instability modelers trying to understand the important mechanisms involved during these important initial periods of instability.

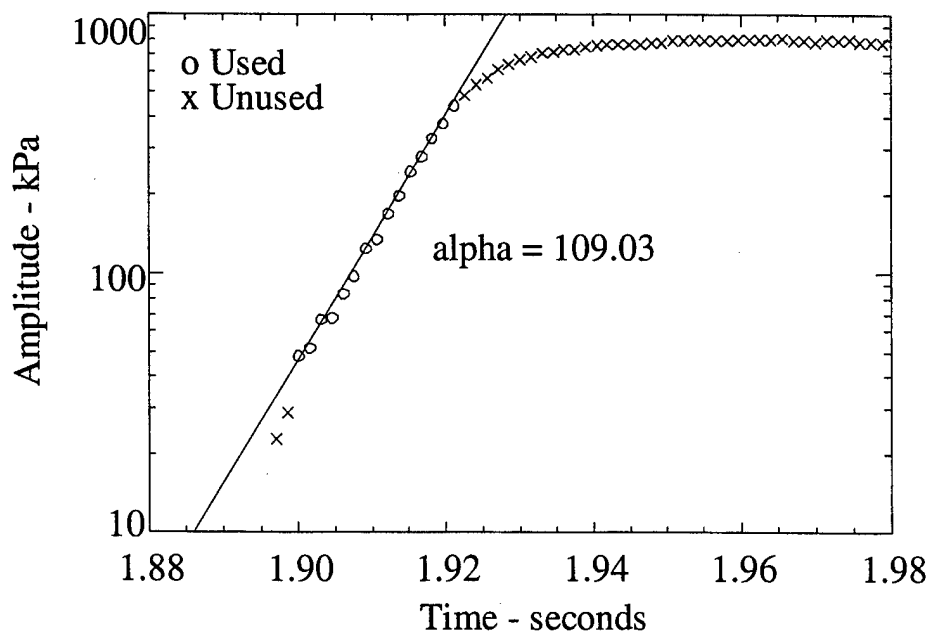


FIGURE 20. Growth Rate of Oscillations From Pulse 2 of Motor No. 4.

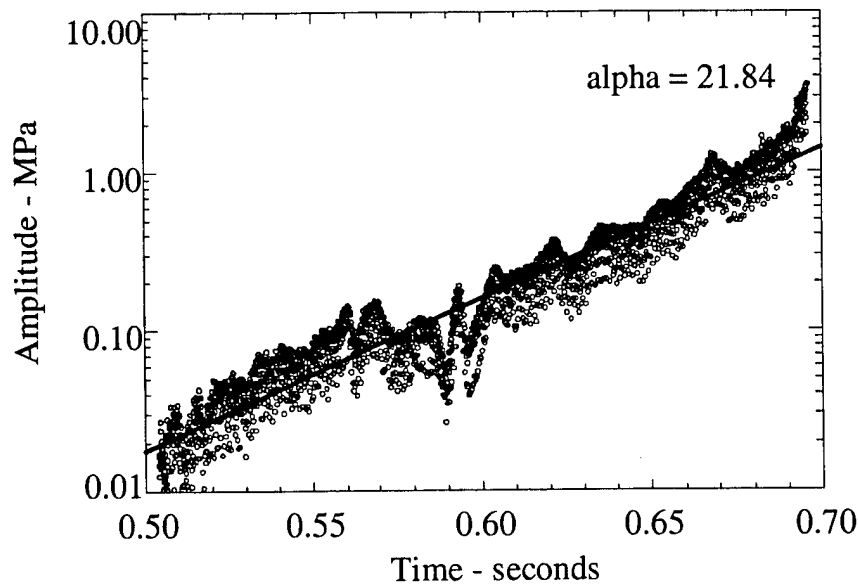


FIGURE 21. Growth Rate of Spontaneous Tangential Oscillations of Motor No. 5.

Nonlinear Instability. Why does the severity of the oscillations, both the nonlinear longitudinal and tangential, increase as the motor operating pressure is increased? Two possible explanations will be discussed. First, if one examines linear stability theory it is possible to see what driving and damping factors change as pressure is increased in a rocket motor. Table 7 illustrates this point. In this table are the individual terms that make up the linear stability prediction shown in Figure 19 from the SPP/SSP linear stability computer program (References 11 and 12). Velocity coupling is not included because it has a small value and varies little in magnitude. Although the driving due to pressure coupling decreases with pressure, the decrease in combined damping from the flow turning, and especially nozzle damping, more than offsets the pressure coupling decreases and result in a motor that has a much lower margin of linear stability. In fact, the 13.8-MPa motor is more than two times less stable than the 3.45-MPa motor. It is widely held that the nonlinear stability is related to the linear stability (References 1 through 10). The damping changes can be explained in large part by a smaller nozzle opening. This causes a decrease in nozzle damping and a lower mean velocity of the chamber flow when the motor is operated at higher chamber pressures, which reduces the flow turning losses.

Another approach at understanding the effect of pressure in the stability of the motors is to examine what effect pressure has on the acoustic boundary layer and this interaction with the propellant response. A study undertaken by Beddini and Roberts analyzed the response function produced by both pressure coupling and oscillatory crossflow conditions ("velocity response") within the acoustic boundary layer near a propellant surface (References 15, 16, and 17). Their computational results (conducted with several simplifying assumptions) indicated that the velocity response function is of a similar form to that assumed by Baum and Levine and by Levine and Culick, i.e., negligible response below a threshold velocity or pressure amplitude, followed by a

nearly linear dependence on the absolute value of acoustic velocity or pressure amplitude above the threshold (References 18, 19, and 20). The mechanism producing this response was found to be enhanced thermal diffusivity caused by turbulent transition of the acoustic boundary-layer. The velocity response was found to depend on operating conditions such as mean chamber pressure and frequency. As mean chamber pressure was increased, it was found that the local acoustic pressure amplitude required to exceed the threshold condition decreased appreciably (Figure 22). This indicates that a motor that does not exhibit a local velocity response at lower chamber pressures may experience a significant nonlinear response (in comparison with pressure coupling) at elevated chamber pressures. According to Beddini, this type of response might require additional damping sources at elevated chamber pressures to ensure motor stability. Figure 23 shows a representation of the nonlinear response variation with acoustic velocity levels at three motor pressures. The higher the pressure the lower the threshold velocity and the higher the response at a particular acoustic oscillatory level. In addition, as motor pressure is increased the mean velocity in the motor goes down, pushing the operating condition farther to the right and increasing the nonlinear response of the propellant. Increasing pulse amplitude will also cause an increase in the response.

TABLE 7. Linear Driving and Damping Terms as a Function of Pressure.

Web, mm	Total alpha, 1/sec			PC coupling, 1/sec			Nozzle damping, 1/sec			Flow turning, 1/sec		
	3.45 MPa	10.3 MPa	13.8 MPa	3.45 MPa	10.3 MPa	13.8 MPa	3.45 MPa	10.3 MPa	13.8 Mpa,	3.45 MPa	10.3 MPa	13.8, MPa
0.25	-203.17	-115.01	-102.89	151.91	86.32	77.29	-239.07	-135.67	-121.51	-113.30	-64.21	-57.53
2.54	-189.39	-99.50	-85.36	143.00	75.10	64.42	-224.62	-117.88	-101.11	-105.99	-55.59	-47.68
5.08	-169.79	-88.96	-76.38	128.86	67.52	57.96	-202.22	-105.89	-90.90	-95.14	-49.79	-42.74
7.62	-152.70	-79.57	-68.30	116.42	60.65	52.06	-182.51	-95.05	-81.59	-85.64	-44.58	-38.27
10.2	-137.94	-71.60	-61.44	105.53	54.75	46.98	-165.32	-85.76	-73.59	-77.41	-40.15	-34.45
12.7	-125.96	-65.19	-55.93	93.15	48.18	41.33	-148.17	-76.63	-65.74	-70.31	-36.36	-31.20
15.2	-114.73	-59.25	-50.82	85.40	44.07	37.80	-135.57	-69.97	-60.01	-64.08	-33.07	-28.37
17.8	-104.89	-54.07	-46.40	78.51	40.44	34.71	-124.42	-64.10	-55.01	-58.62	-30.20	-25.92
20.3	-96.22	-49.56	-42.52	72.37	37.26	31.96	-114.50	-58.96	-50.57	-53.79	-27.70	-23.76
22.9	-88.54	-45.62	-39.25	66.89	34.45	29.63	-105.67	-54.43	-46.82	-49.52	-25.51	-21.95
25.4	0.00	0.00	0.00	0.00	0.00	0.00	0.00	0.00	0.00	0.00	0.00	0.00

In recent unpublished studies by the author, that applied the nonlinear model of Levine and Baum discussed above, increasing pressure did not tend to increase a motor's susceptibility to nonlinear combustion instability (References 18 and 19). However in this study, the threshold velocity was assumed to be zero and the nonlinear velocity coupled response was held constant with pressure. It is the understanding of the author that the nonlinear velocity coupled response is a strong function of pressure and not having this dependence in his work yielded incorrect correlations between pressure and combustion instability. Unfortunately, experimental or empirical functional dependencies of threshold velocity and velocity coupling with pressure are currently not available, making exact nonlinear combustion instability predictions difficult. Experiments are needed to evaluate threshold velocities and nonlinear combustion response in order to apply the nonlinear combustion motor stability models and obtain accurate qualitative data.

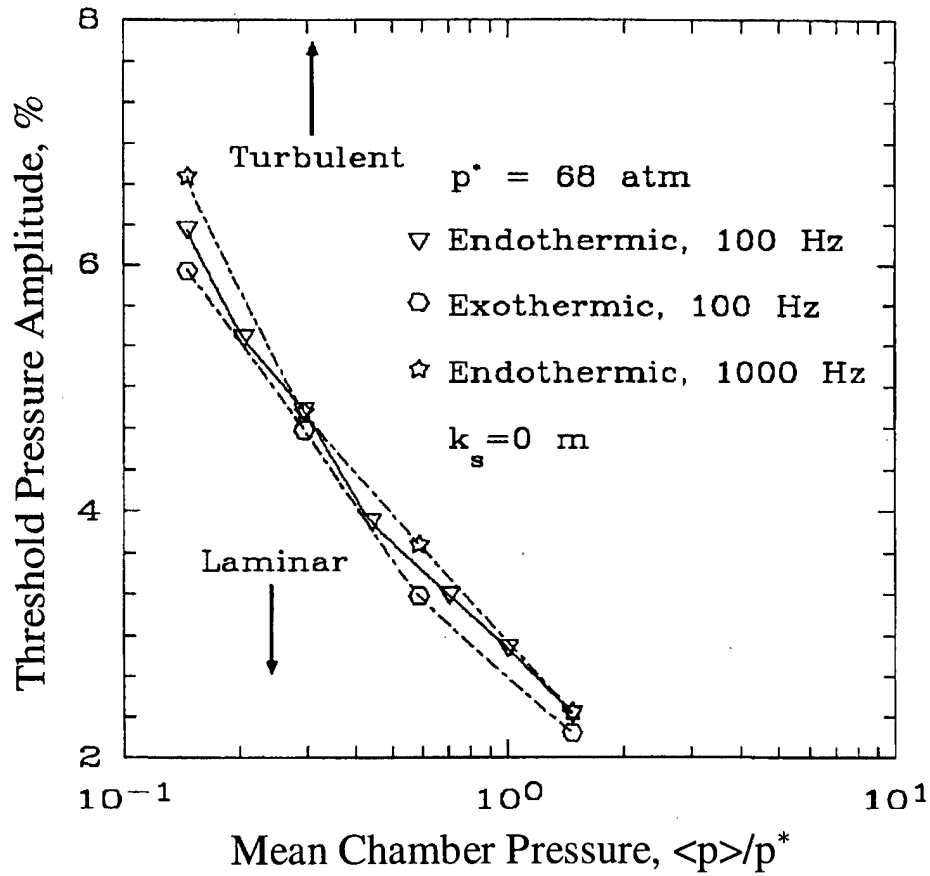


FIGURE 22. Threshold Pressure Amplitude Versus Mean Chamber Pressure.

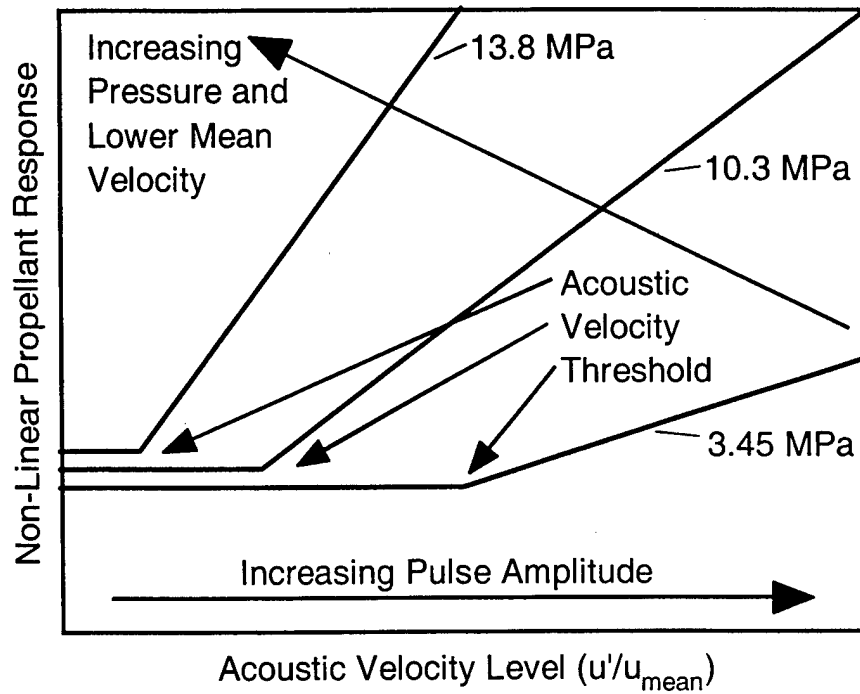


FIGURE 23. Nonlinear Response Variation With Acoustic Velocity and Motor Pressure.

The discussions above are not necessarily opposed to each other and in many cases support each other. They address the problem of instability with differing degrees of sophistication and emphasis. What is important is that they all indicate that increasing pressure can lead to more severe instability in solid rocket motors. It is hoped that by understanding the mechanisms, logical experiments can be performed and parameters can be varied to control combustion instability in motor systems that operate at higher pressures.

FIRING RESULTS AND ANALYSIS OF MOTORS NO. 6 THROUGH 10

Motors no. 6 through 10 were successfully fired during August 1997. Figures 24 through 28 show the DC coupled ballistic pressure of each motor. Included on Figures 24 and 25 are two pressure traces. One is the high frequency DC coupled signal recorded from the Kistler gauges and the other is from the low frequency strain gauge type transducer, which indicates the actual pressure level in the motor. Both were included to illustrate that although piezoelectric gauges yield excellent AC data, their DC data are not as good due to drifting of the gauge with time. Detailed plots shown later will indicate the true AC noise levels and show much greater detail of the pulses. The behavior of each motor fired is summarized below.

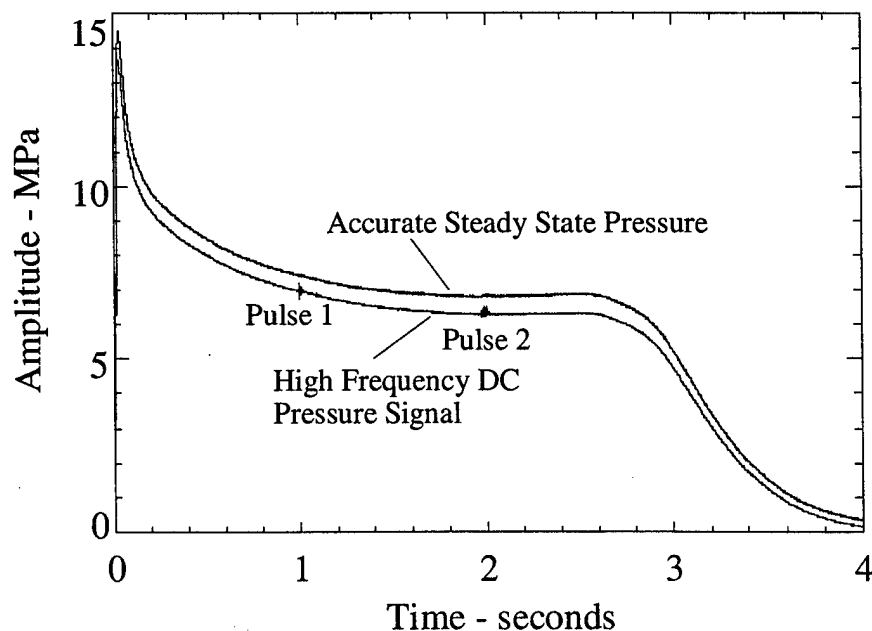


FIGURE 24. Motor No. 6 Ballistic Pressure.

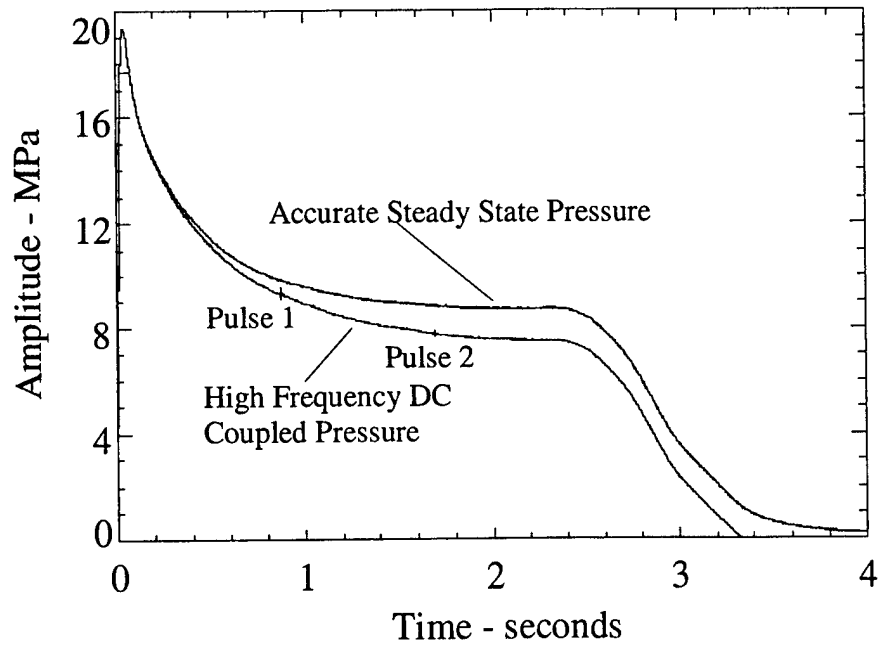


FIGURE 25. Motor No. 7 Ballistic Pressure.

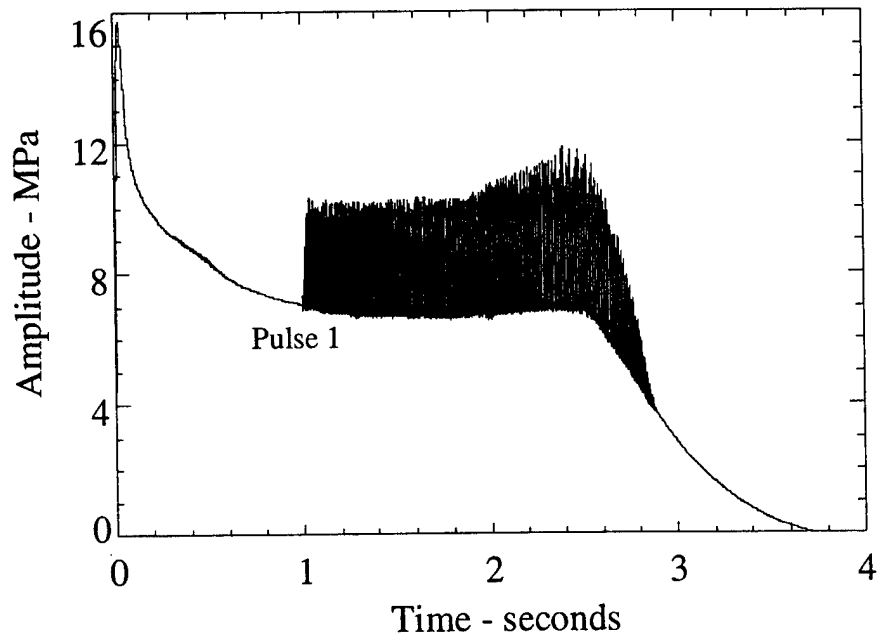


FIGURE 26. Motor No. 8 Ballistic Pressure.

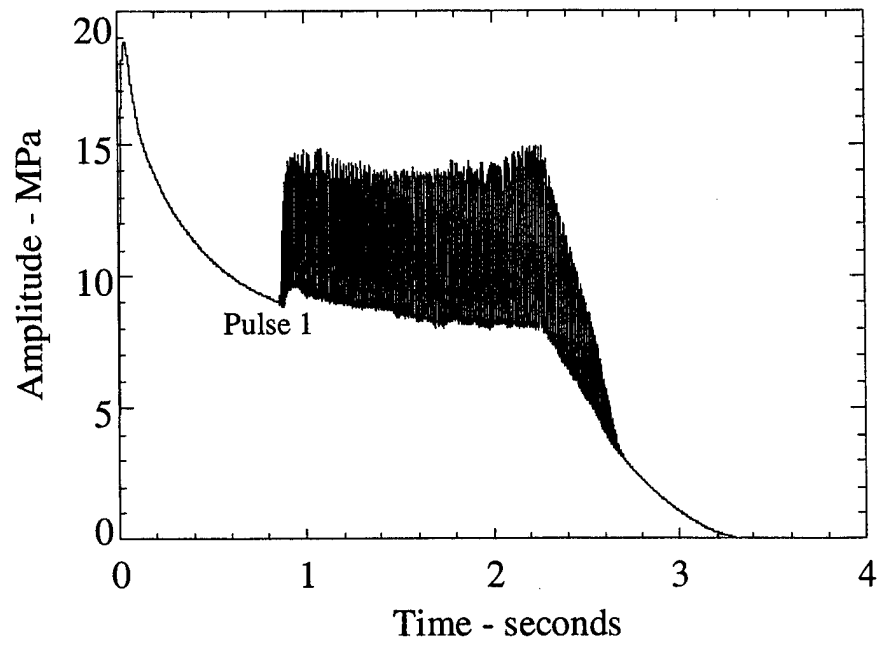


FIGURE 27. Motor No. 9 Ballistic Pressure.

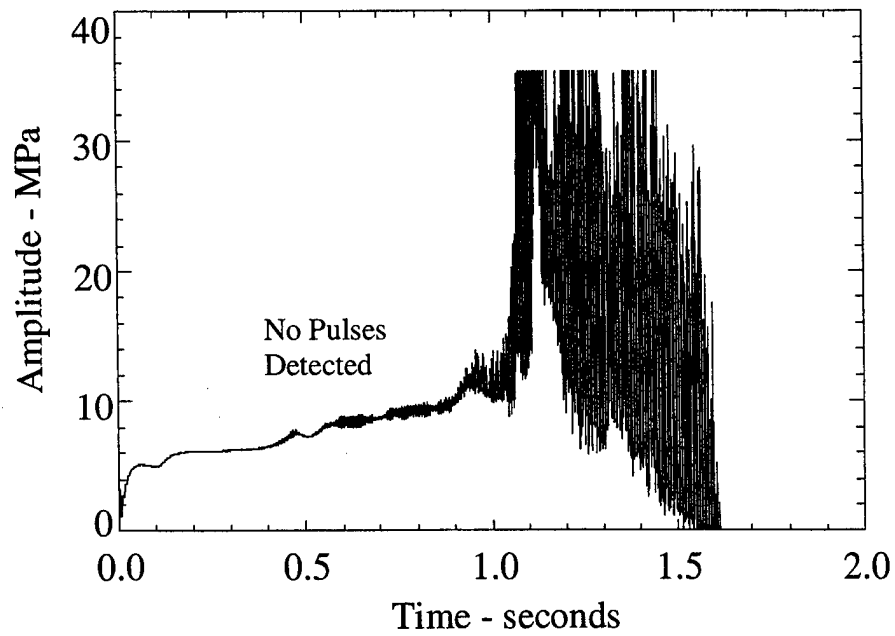


FIGURE 28. Motor No. 10 Ballistic Pressure.

Motor No. 6. Motor no. 6 had a chamber pressure of 6.9 Mpa and star aft geometry, and was loaded with propellant "A." It was pulsed twice lightly at 3.9 and 3.1% levels (276 and 205 kPa, respectively) and both pulses decayed, i.e. no oscillations resulted.

Motor No. 7. Motor No. 7 had a chamber pressure of 10.3 Mpa and star aft geometry, and was loaded with propellant "A." It was also pulsed twice lightly at 4.7 and 2.9% levels (442 and 220 kPa, respectively) and both pulses decayed.

Motor No. 8. Motor No. 8 had a chamber pressure of 6.9 Mpa and star aft geometry, and was loaded with propellant "A." This motor was pulsed hard at 9.7% (689 kPa). The motor went into violent nonlinear longitudinal oscillations, i.e. the oscillations grew to a limiting amplitude and the chamber pressure was elevated.

Motor No. 9. Motor No. 9 had a chamber pressure of 10.3 Mpa and star aft geometry, and was loaded with propellant "A." This motor was pulsed hard at 10.2 percent (959 kPa). The motor went into violent nonlinear longitudinal oscillations.

Motor No. 10. Motor No. 10 had a chamber pressure of 13.45 Mpa and full cylinder geometry, and was loaded with propellant "B." This motor went spontaneously unstable before pulsing occurred, and experienced large DC pressure shifts and reached chamber pressures in excess of 41 MPa before the nozzle insert was ejected.

Table 8 contains specifics on the pulsing results. Examining the normalized pulse column, it can be seen that the actual pulsing levels compare quite favorably with the estimated pulse amplitudes. For motors no. 3, 4, and 5 the pulsing agreement was not as good (see Table 6). Figure 29 shows the AC data for pulse 2 of motor no. 6. This was an interesting pulse as it appeared that the motor almost went unstable. In this figure, some of the dark area immediately after the pulse is probably transducer ringing due to the explosive pulse. Figure 30 shows the DC data for pulse 1 of motor no. 8. The pulse and resultant oscillations are nonlinear and steep fronted. In approximately 11 cycles, the oscillations reached a limiting amplitude of around 3.5 MPa. The limiting amplitude eventually increased to a value of 5.5 Mpa, as can be see in Figure 31, showing all AC data for motor no. 8. Figure 32 shows some tangential oscillation detail toward the beginning of motor no. 8 and marked in Figure 31. These oscillations are low in magnitude but do contain frequencies and frequency shifts indicative of tangential oscillations. The following sections will describe some of the observations of the motor firings. Included will be discussions on stability boundaries, stability additives, waveform shape and phase relationships, frequency content, and motor no. 10 failure analysis.

Stability Boundaries. One aspect looked for in past motor firings was the pulsing level required to trigger a motor into nonlinear instability. In motor no. 6, a 3.9% pulse did not trigger the motor. A 9.7% pulse in an identical motor no. 8 did. This behavior was repeated in the higher pressure motors no. 7 and 9, which had 4.7 and 10.2% pulses, respectively. Figure 33 shows this graphically by comparing the steady state gauge outputs for motors no. 6 and 8, and motors no. 7 and 9, respectively. The steady state strain gauge type transducer does not have the frequency response and, hence, the oscillatory levels shown by the gauge are much lower than they actually were, as was

indicated in Figures 26 and 27. These gauges were used in Figure 33 for clarity, making the effects much easier to see. This type of data is very hard to obtain and will be very valuable in gaining understanding into the physics of combustion instability. A qualitative knowledge of what pulsing level is required to trigger a motor into limiting amplitude nonlinear instability should provide insight into the mechanistic behavior of this form of instability. Figure 34 shows real time photographs of motors no. 7 and 9 taken at the same time during burn after the onset of oscillation of motor no. 9. The difference is obvious. The bottom motor in Figure 34 experiencing instability has a much brighter plume signature.

TABLE 8. Summary of Pulse Data for Motors No. 6 Through 10.

Motor no.	Pulse no.	Parameter							
		Chamber pressure, Mpa	Est pulse, kPa	Pulse amp, kPa	Normalized Pulse, % (planned)	Time, sec	Measured alpha, 1/sec	DC pressure, Mpa	Limited amplitude, Mpa
6	1	7.1	355	276	3.9 (5.0)	1.0	-125	---	---
	2	6.6	197	205	3.1 (3.0)	2.0	-92	---	---
7	1	9.4	535	442	4.7 (5.0)	0.865	-87	---	---
	2	7.6	306	220	2.9 (3.0)	1.715	-50	---	---
8	1	7.1	710	689	9.7 (10.0)	1.0	---	0.69	5.52
9	1	9.4	1069	959	10.2 (10.0)	0.865	---	1.38	6.90
10	1	10.7	345	---	---	0.97	---	> 28	> 35

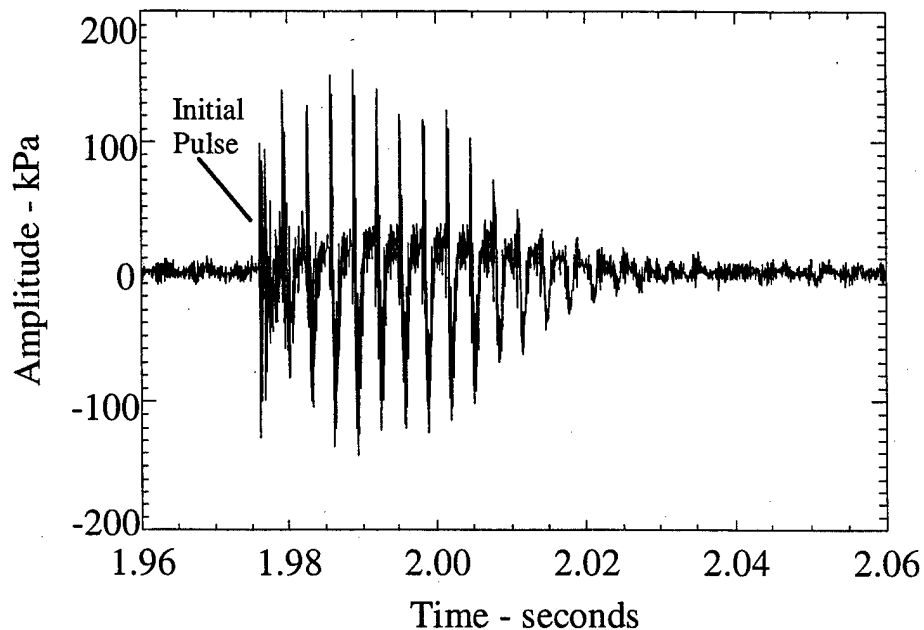


FIGURE 29. Details of Pulse 2 of Motor No. 6, AC Data.

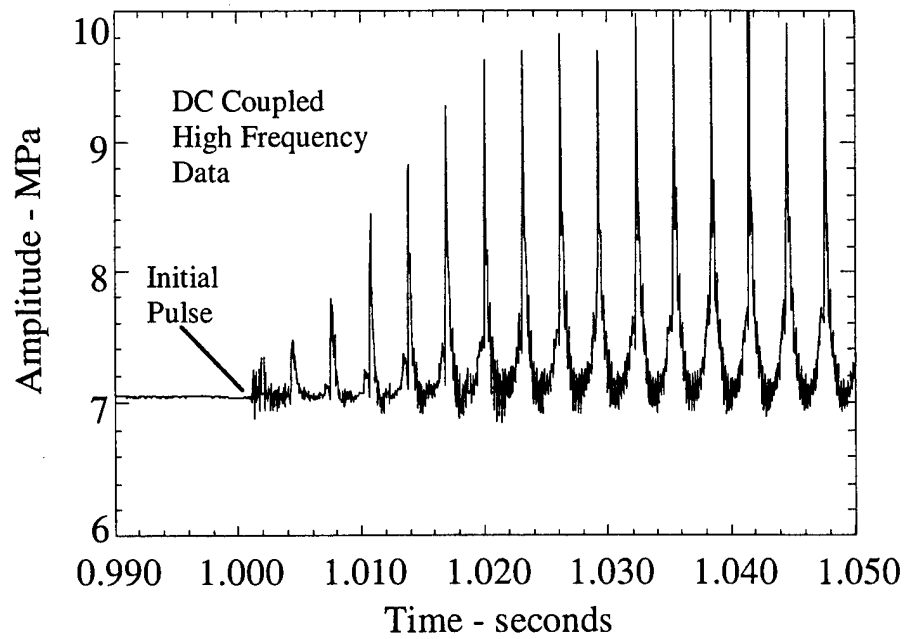


FIGURE 30. Details of Pulse 1 of Motor No. 8, DC Coupled Data.

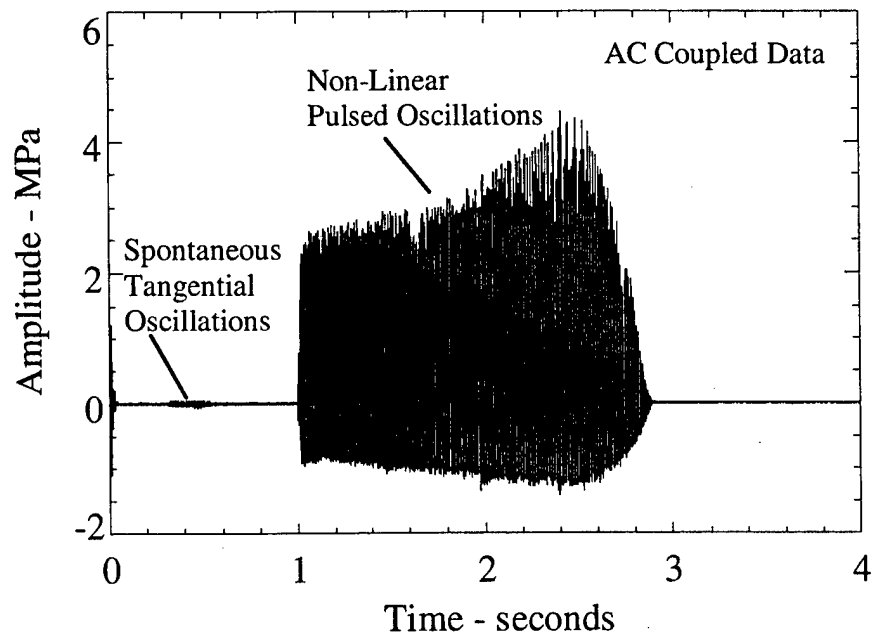


FIGURE 31. AC Coupled Data of Motor No. 8.

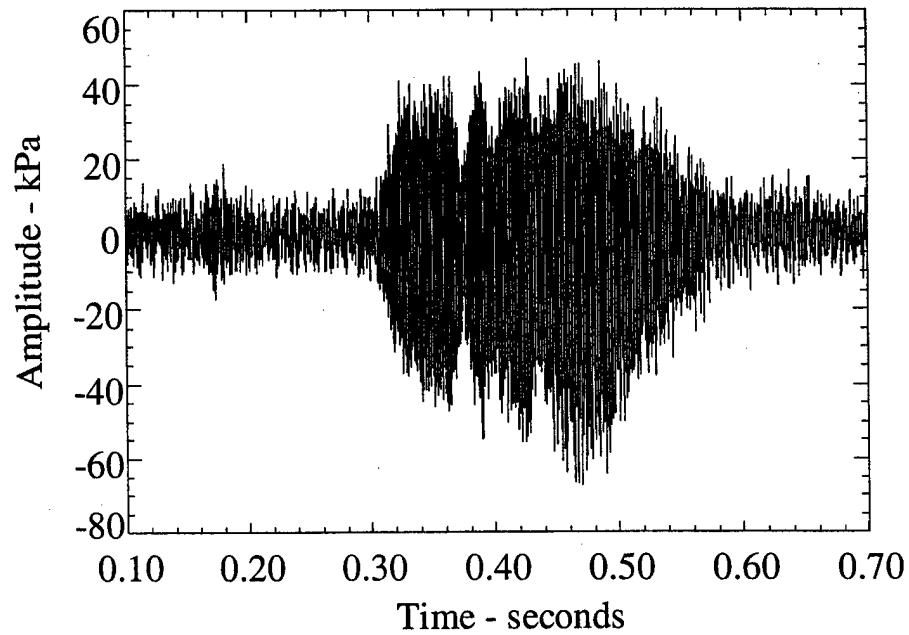


FIGURE 32. Low Level Spontaneous Tangential Oscillations of Motor No. 8.

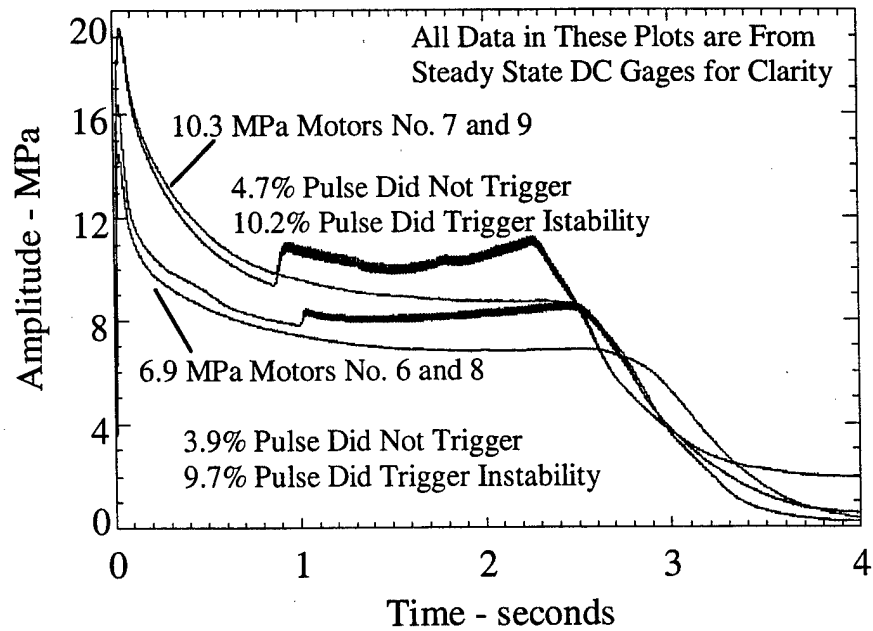


FIGURE 33. Examples of Pulsing Threshold.

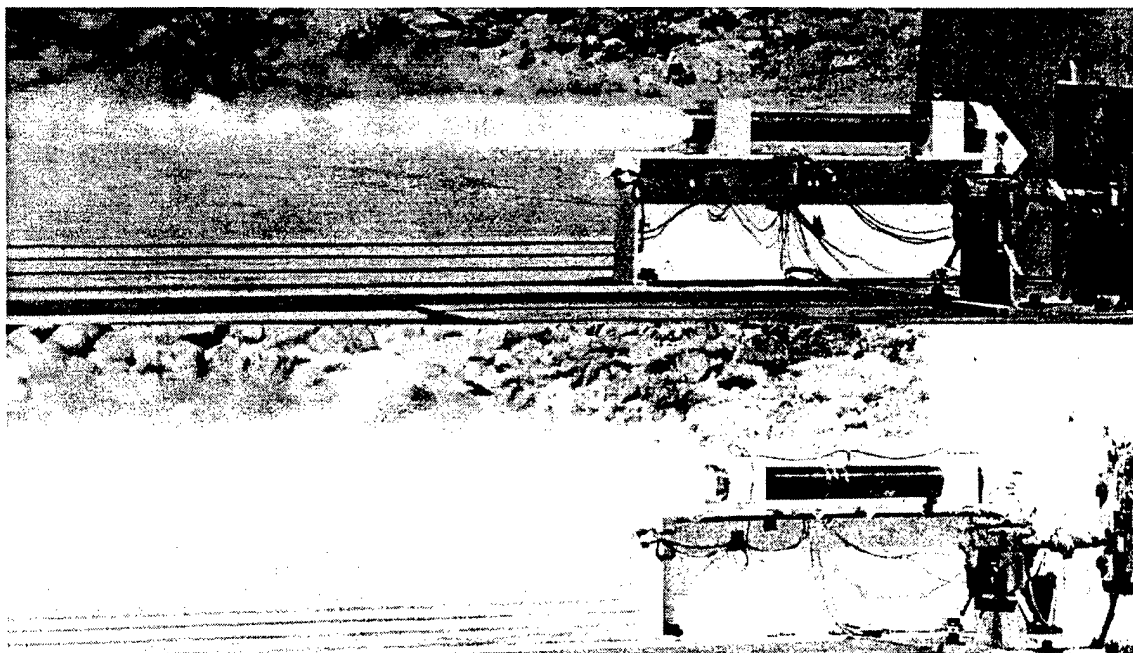


FIGURE 34. Comparison of Motors No. 7 and 9.

Stability Additives. In past motor pulsing activities it was very difficult to pulse motors into nonlinear instability when the propellant contained stability additives (Reference 2). Motors no. 6 through 9 in this study had propellants that did have a stability additive, 1 % ZrC. Motors no. 8 and 9 were both pulsed into instability with approximately 10% pulse levels. Although the exact propellant in the past studies was slightly different, the geometry, pressure, and pulse magnitudes were not. In the past studies, when the motors without additives did go unstable, the resulting oscillations were often very hard with large DC pressure shifts. In motors in this study, the oscillations were hard, often exhibiting 5- to 7-MPa peak-to-peak oscillations. In some of the past motors without stability additives, the oscillatory levels were also near 7 MPa. However, the DC shifts in this study were much smaller, on the order of 1 MPa for the 6.9-MPa motor and 2 MPa for the 10.3-MPa motor. The past motors of similar geometry and operating pressure, but without stability additive, had DC shifts of 5 to 8 MPa. The presence of a stability additive may have the effect of reducing the DC shift once a motor does go unstable.

The motors in the past study containing stability additives were pulsed with similar and sometimes stronger pulses and yet did not go unstable. As mentioned above, one difference was the propellant. Although both were AP/HTPB reduced smoke propellants of similar rate and exponent, there was one important difference. The current propellant contained 4% RDX. The presence of RDX, making these motors more susceptible to pulsing, is very speculative and more research should be performed.

Waveform Shape and Phase Relationships. By installing three gauges along the axis of the motor, it was hoped to gain insight into the phase, waveform shape, and frequency content of the acoustic oscillations. Figure 35 shows some of this detail. The onset of oscillations is shown for motor no. 9 for all three high-frequency gauges. All three gauges were mounted very close to the motor cavity, with no loss in signal response

at the 20-KHz sample rate. To allow more readable comparison of the signals, the middle signal in Figure 35 has an artificial offset of 3 MPa and the aft signal has an offset of 6 MPa. The gauges all use the identical time scale, making phase relationships possible. It is quickly noted that the aft gauge is 180 degrees out of phase with the forward gauge. The middle gauge is 90 degrees out of phase. The middle gauge also appears to have dominant harmonics at twice the frequency and half the amplitude, compared to the forward location. This is expected because the oscillatory wave passes the mid-point twice for each cycle of oscillation. Because most of the longitudinal acoustic energy is conserved for a cycle of oscillation, the energy level or amplitude is half of the amplitudes at the ends of the motor. Also seen in this figure is the relative noise level before the onset of oscillations. Typical noise levels were sometimes less than 7 kPa out of 35 MPa.

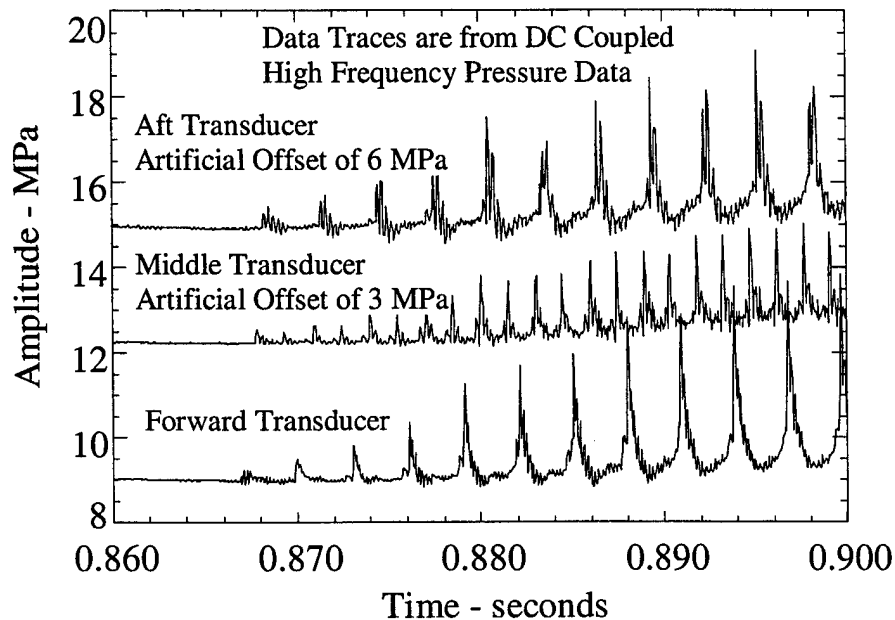


FIGURE 35. Waveshape Comparison for Motor No. 9.

Frequency Content. The frequency content of acoustic oscillations of motor no. 9 can be seen in Figure 36. These are fast Fourier transform (FFT) plots of oscillations of the motor at the forward, middle, and aft locations at around 2 seconds after the onset of pulsed instability. Twenty-eight harmonics of the first longitudinal mode can be seen. The second harmonic and subsequent even harmonics are the dominant ones at the middle location. Also, the level of the oscillations is roughly half that of the forward and aft ends. This is expected based on the observed middle pressure signal in Figure 35.

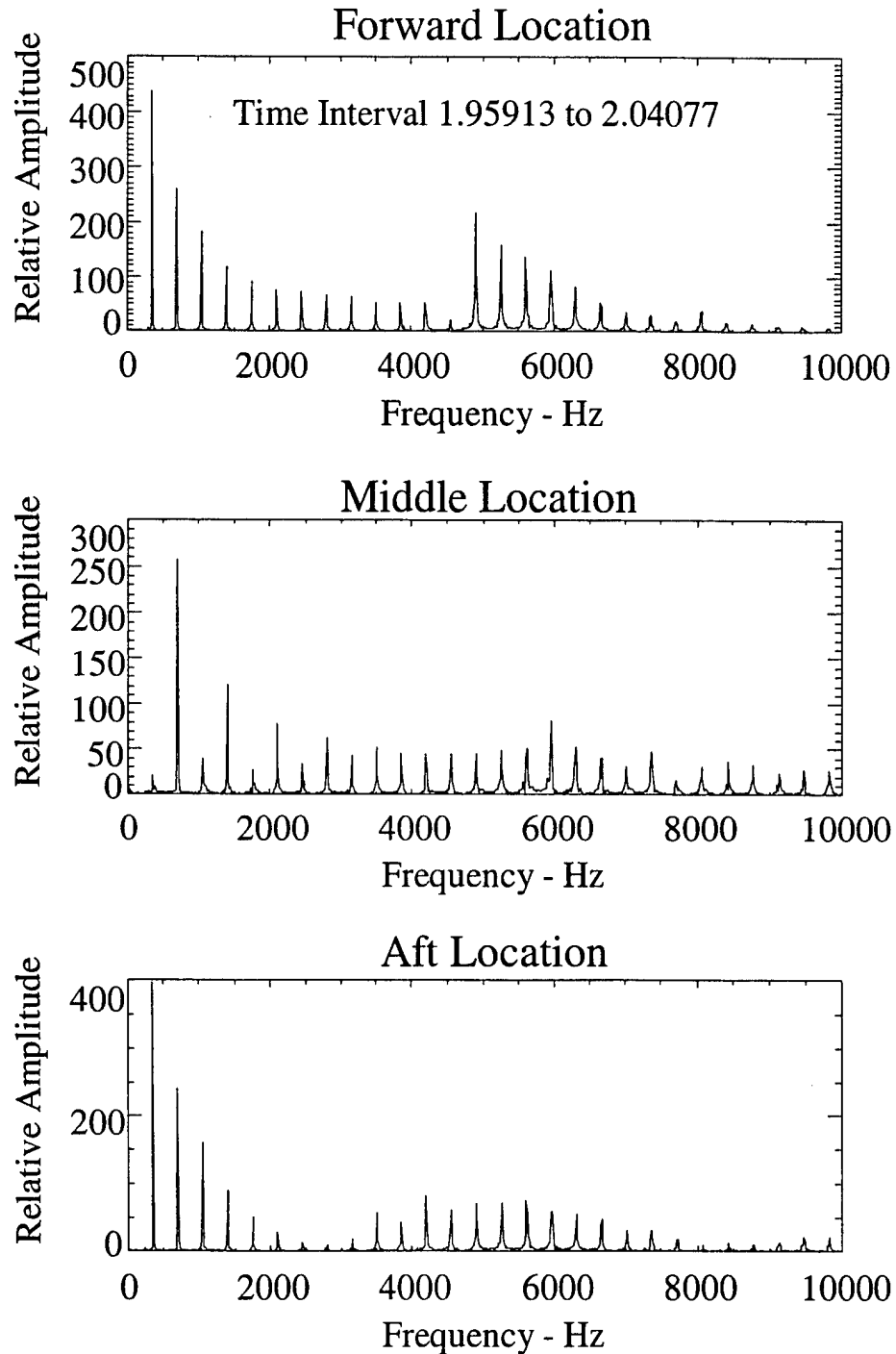


FIGURE 36. Frequency Analysis Comparison of Motor No. 9.

The increase in magnitude of the modes around 6,000 Hz is due to coupling between the longitudinal waveforms and the tangential modes of the motor, as discussed above and shown in Figure 8 and 9. These have been seen in past motor firings as well (References 1 through 4); however, the observed frequency content of the tangential modes at the three axial locations is different. In Figure 36, the forward end frequency

peaks around 5,000 Hz corresponds to the tangential mode of the case inner diameter. To explain this more fully, there is a 2.5-cm portion of exposed case wall at the forward end of the motor to allow the pulses to be introduced into the motor chamber. The exposed end face of the propellant was inhibited. The observed frequency at the forward end is approximately the computed first tangential mode of the inner case diameter. Using Equation 1, a value of 4,970 Hz is computed. This mode remains roughly constant as the motor burns. Looking at the tangential oscillations at the middle shows the dominant frequency to be about 6,000 Hz. This corresponds to the estimated frequency using Equation 1 for the inner diameter of the motor at the middle. As expected, this peak does decrease in frequency, as the motor burns and the inner diameter of the motor increases. The tangential coupling at the aft end, Figure 36, is not as distinct. This may be due to effects of the nozzle and more dominant star geometry in the aft end. However, it is still there. The conclusion reached here is that the dominant nonlinear oscillations appear to couple with whatever the local tangential mode happens to be along the length of the rocket motor. In recent work by Harris, the coupling relationships between various local oscillatory modes motors experiencing high amplitude oscillations was also reported by using very sophisticated data reduction techniques (Reference 21).

Figure 37 is a FFT of the oscillations occurring before the pulse of motor no. 8 at around 0.5 second. Recalling Figures 31 and 32, this time corresponds to tangential oscillations. It was originally thought that the tangential modes were excited by the pulses; however, the tangential oscillations shown here occurred without any apparent external stimuli. In Figure 37, both first and second tangential modes are present. It is interesting to note that the second tangential mode was not observed when the nonlinear longitudinal oscillations occurred (see Figure 36). Finally, Figure 38 is a FFT of motor no. 6 before any pulsing occurs, to examine what low level oscillations might be present. It shows frequency peaks near the first and second tangential modes. It is assumed that the multiple peaks corresponding to the first tangential mode around 4,000 Hz are because the mode is very weak and probably not organized like the stronger tangential modes shown earlier in Figure 37. Notice that the magnitude of oscillations is much lower than those in Figures 36 and 37. The bulge around 200 Hz is believed to be caused by some 60-cycle noise causing peaks at 60, 120, 180 Hz, etc.

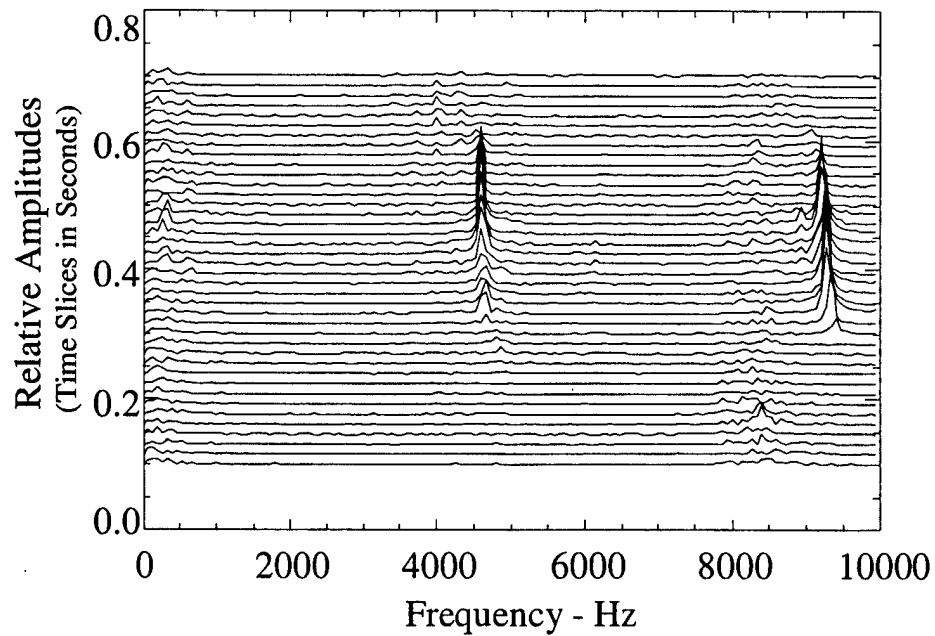


FIGURE 37. Frequency Analysis of Motor No. 8 From 0.1 to 0.7 Second.

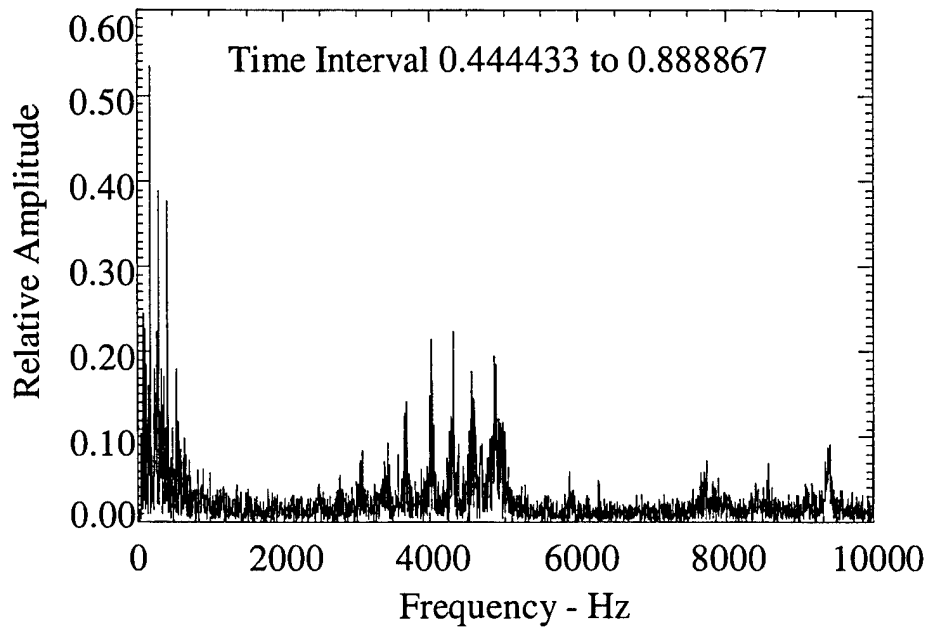


FIGURE 38. Frequency Analysis of Motor No. 6 Before Pulsing.

Motor No. 10 Failure Analysis. Motor no. 10 was a 10.3-MPa full cylinder with a propellant containing no stability additive and was to be pulsed at 5 and 3% levels. Three

high-frequency Kistler gauges were mounted at the forward, middle, and aft ends of the motor. This was supposed to be a repeat of motor no. 4 of the previous year in which the motor was stable to the first pulse and unstable to the second. The difference was enhanced instrumentation with the three gauges. Unfortunately, the motor went spontaneously unstable at about 1 second with the first tangential mode. This was followed by a DC shift in pressure to 41 MPa. At this elevated pressure, the nozzle insert was ejected and the middle and aft gauges blew off and were lost. However, good data were obtained up to this point. Figure 39 is a photograph taken during the firing, after the gauges were lost. Notice the two vertical plumes where the transducers were located. Despite the failure, the case will be refurbished and reused. Figures 40 and 41 show the steady state pressure and oscillatory pressure of the motor, respectively. Figure 42 shows a FFT waterfall plot of the entire firing. It is clearly seen from this figure that the motor experienced a tangential mode, which led to excessive DC pressure shifts and motor failure. Examining the other two AC gauges mounted at the mid-point and aft end showed similar behavior except they had much higher oscillatory amplitudes. Figure 43 shows this behavior by plotting all three gauges over a very short time period. Artificial offsets were added to the middle and aft pressure traces to allow easier visualization of the data. Although the noise level is very low, the resolution of the signal is poor because of the low sample rate, 20,000 Hz, compared to the frequency of the mode, 6,000 Hz. This is only about 3 points per cycle. The long period oscillations are probably due to dithering of the signal because of the low sample rates. However, it is interesting to note that the magnitude of the oscillations is much higher at the middle and aft locations. It is assumed that this is because the tangential oscillations are combustion driven, and because no propellant is located very near the forward gauge, the oscillations are lower there. Apparently, the magnitude of the tangential oscillations is very dependent upon the axial position in the motor.

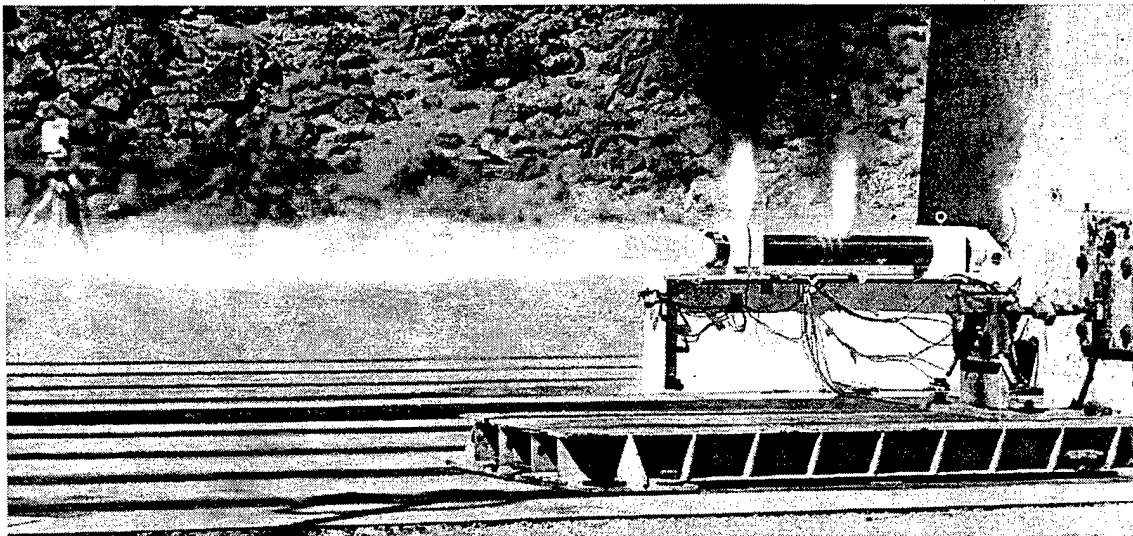


FIGURE 39. Motor No. 10 After Gauge Failure.

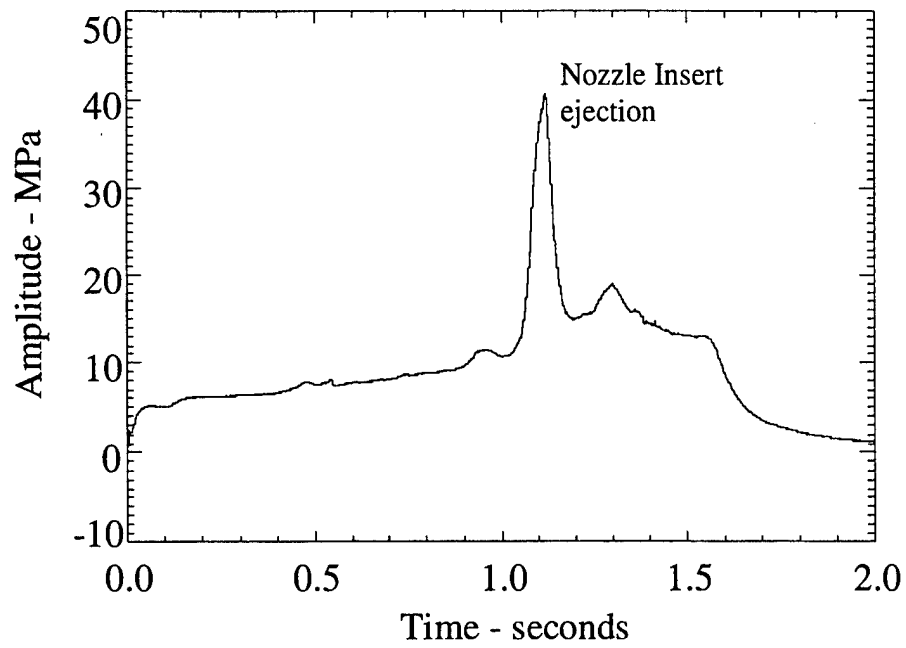


FIGURE 40. Steady State Pressure of Motor No. 10.

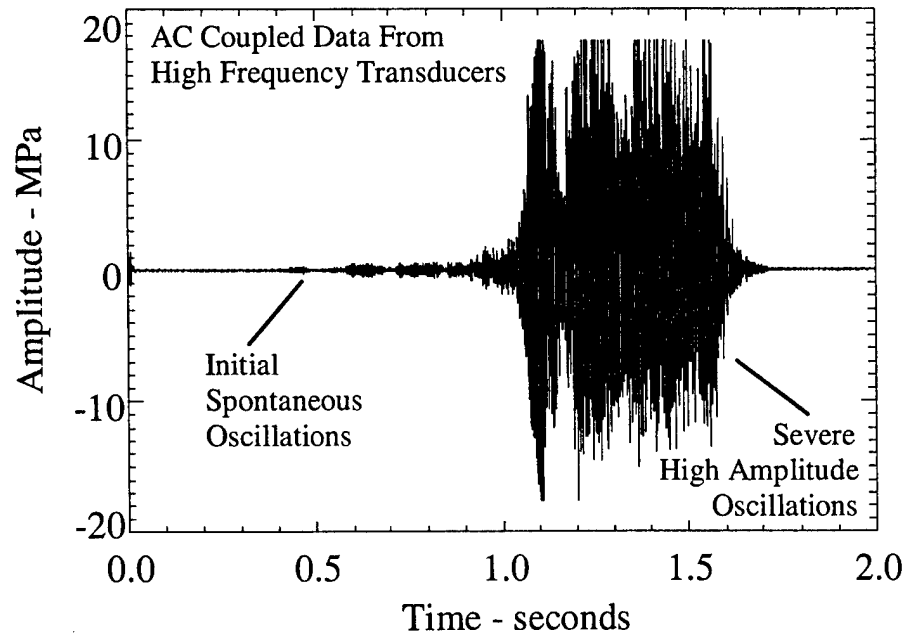


FIGURE 41. High-Frequency Data of Motor No. 10.

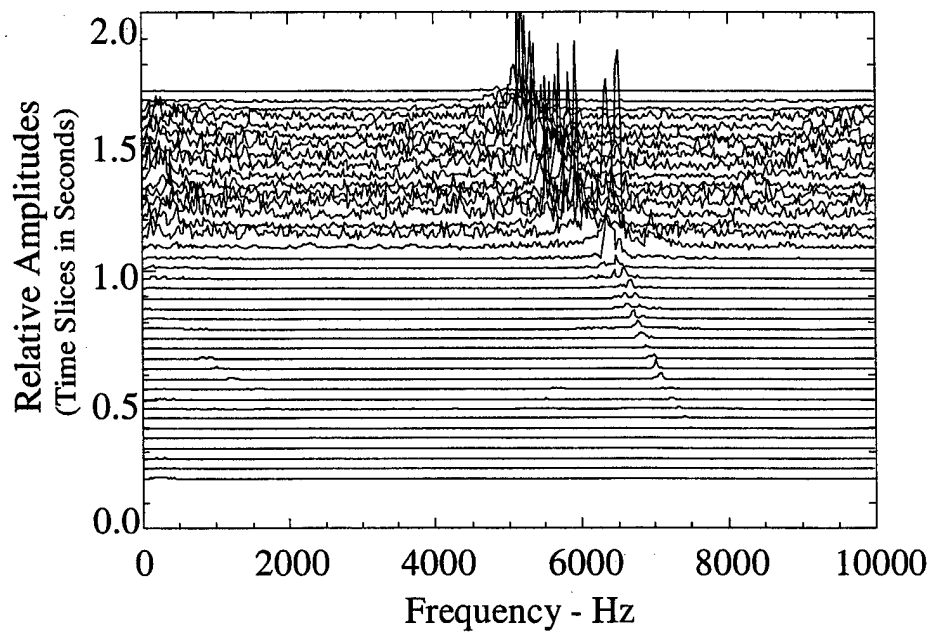


FIGURE 42. Frequency Analysis of Motor No. 10.

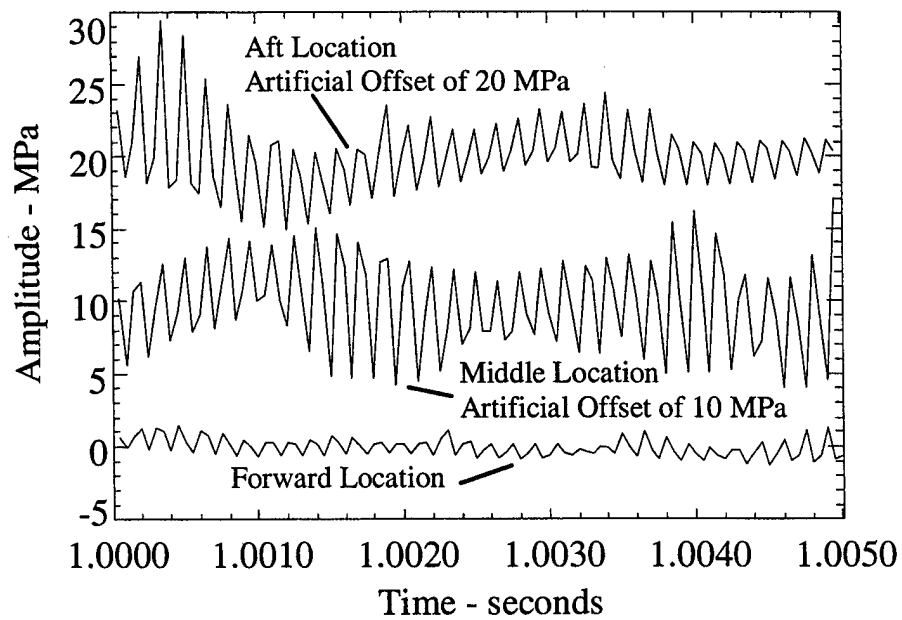


FIGURE 43. Waveshape Comparison for Motor No. 10.

CONCLUSIONS

The purpose of this study was to examine the stability of motors as a function of pulse amplitude, geometry, pressure and propellant formulation. Ten motors with extensive instrumentation to characterize their combustion instability behavior were carefully fired and pulsed. Several significant observations were made from the data.

(1) The susceptibility of a motor to go unstable with pressure was shown in a very clear and precise manner. As pressure was increased, it was easier to pulse a motor unstable. Also the inherent stability of the motors decreased with pressure.

(2) Comparisons with the predicted stability were performed with favorable results. Both the magnitude and trends in the data agreed with the theoretical predictions.

(3) Linear growth rates were observed for both the pulsed longitudinal and spontaneous tangential instabilities.

(4) The triggering level was bracketed between two pulse amplitudes for two sets of motor firings at different pressures.

(5) The function of additives to suppress triggered instability was questioned. It was possible to trigger two motors that used stability additives in their propellant. The motors that did go unstable showed lower than expected DC pressure shifts, which may be due to the additive. In addition, the DC shifts appeared to increase slightly as motor pressure increased.

(6) Detailed acoustic waveform measurements were performed by mounting transducers at three locations along the length of the motor. It showed the expected phase, frequency, and amplitude characteristics as a function of axial location along the motor. Details of these data are available. It should also be mentioned that the noise level for some of the data was less than 7 kPa out of 35 Mpa (1 psi out of 5,000).

(7) Extensive frequency analysis was performed on the nonlinear, tangential, and background oscillations. One important conclusion reached here is that the dominant nonlinear oscillations appear to couple with whatever the local tangential modes happen to be.

(8) Detailed analysis was performed on motors no. 5 and 10, which failed. It was concluded that spontaneous tangential oscillations caused the over-pressurization in both motors.

(9) Another important lesson learned in this study is the destructive and potentially violent nature of a motor experiencing combustion instability. The motor tie downs for motor no. 5 were designed with a safety factor of 10 times the expected thrust of 35 kN. The actual thrust achieved reached over 400 kN, or nearly 12 times higher. The presence of instability made things even worse. If motor no. 5 had merely failed due to nozzle blockage, without combustion instability, it is most likely that the motor would merely

have burned to completion after ejecting the blockage. The thrust oscillations acted like a jackhammer to cut the retaining bolts. Motor tie down hardware was redesigned with limits in excess of the absolute worst case scenario.

(10) An added important result of this work has been a working knowledge of dealing with higher pressure motors in terms of instrumenting, pulsing, and fabricating motor hardware to allow detailed measurements to be made.

It is hoped that the data provided here, and future and past data, will provide other researchers acoustic oscillatory data for model validation purposes and insight into the physical mechanisms that cause this type of combustion instability.

REFERENCES

1. F. S. Blomshield, J. E. Crump, H. B. Mathes, R. A. Stalnaker, and M. W. Beckstead. "Stability Testing of Full-Scale Tactical Motors," *AIAA J. Propulsion and Power*, Vol. 13, No. 3 (May-June 1997), pp. 349-355.
2. F. S. Blomshield, H. B. Mathes, J. E. Crump, C. A. Beiter, and M. W. Beckstead. "Nonlinear Stability Testing of Full-Scale Tactical Motors," *AIAA J. Propulsion and Power*, Vol. 13, No. 3 (May-June 1997), pp. 356-366.
3. F. S. Blomshield, C. J. Bicker, and R. A. Stalnaker. "High Pressure Pulsed Motor Firing Combustion Instability Investigations," AIAA Paper 97-3253 (July 1997).
4. F. S. Blomshield and R. A. Stalnaker. "Pulsed Motor Firings: Pulse Amplitude, Formulation and Enhanced Instrumentation," AIAA Paper 98-3557 (July 1998).
5. W. G. Brownlee. "Nonlinear Axial Combustion Instability in Solid Propellant Motors," *AIAA J.*, Vol. 2 (February 1964), pp. 275-284.
6. Air Force Rocket Propulsion Laboratory. *Limiting Amplitude Analysis*, by R. C. Jensen and M. W. Beckstead, Hercules, Inc., Magna, UT. Edwards Air Force Base, California, July 1973. (AFRPL-TR-73-61, publication UNCLASSIFIED.)
7. J. D. Baum, J. N. Levine, and R. L. Lovine. "Pulse-Triggered Instability in Solid Rocket Motors," *AIAA J.*, Vol. 22, No.10 (October 1984), pp. 1413-1419.
8. J. D. Baum and J. N. Levine. "Modeling of Nonlinear Longitudinal Instabilities in Solid Rocket Motors," *Acta Astronautica*, Vol. 13, No. 6-7 (June-July 1984), pp. 339-348.
9. J. D. Baum, J. N. Levine, and R. L. Lovine. "Pulsed Instability in Rocket Motors: A Comparison Between Predictions and Experiments," *J. Propulsion and Power*, Vol. 4, No. 4 (July-August 1988), pp. 308-316.
10. P. G. Harris, A. Champlain, and C. Bourque. "Pulse-Triggered Nonlinear Instability in Solid Rocket Motors: An Experimental Study," AIAA Paper 97-3246 (July 1997).
11. Air Force Rocket Propulsion Laboratory. *A Computer Program for the Prediction of Solid Propellant Rocket Motor Performance (SPP)*, Vol. 5, by R. W. Hermsen, J. T. Lamberty, and R. E. McCormick. Edwards Air Force Base, California, September 1984. (AFRPL-TR-84-03661, publication UNCLASSIFIED.)
12. Air Force Rocket Propulsion Laboratory. *Standard Stability Prediction Program for Solid Rocket Motors*, by G. R. Nickerson, F. E. C. Culick, and L. D. Dang. Edwards Air Force Base, California, September 1983. (AFRPL-TR-83-017, publication UNCLASSIFIED.)

13. Air Force Rocket Propulsion Laboratory. *T-Burner Testing of Metallized Solid Propellants*, by F. E. C. Culick. Edwards Air Force Base, California, October 1974. (AFRPL-TR-74-28, publication UNCLASSIFIED.)
14. Naval Weapons Center. "Combustion Instability in Minimum Smoke Propellants," by J. E. Crump. China Lake, CA, NWC, November 1977. (NWC TP 5936, publication UNCLASSIFIED.)
15. R. A. Beddini and T. A. Roberts. "Turbularization of an Acoustic Boundary Layer on a Transpiring Surface," *AIAA J.*, Vol. 26, No. 8 (August 1988), pp. 917-923.
16. T. A. Roberts and R. A. Beddini. "A Comparison of Acoustic and Steady-State Erosive Burning in Solid Rocket Motors," AIAA Paper 89-2664 (July 1989).
17. R. A. Beddini and T. A. Roberts. "Response of Propellant Combustion to a Turbulent Acoustic Boundary Layer," *AIAA J. Propulsion and Power*, Vol. 8, No. 2 (March-April 1992), pp. 290-296.
18. J. D. Baum and J. N. Levine. "Numerical Techniques for Solving Nonlinear Instability Problems in Solid Rocket Motors," *AIAA J.*, Vol. 20 (1982), pp. 955-961.
19. Air Force Rocket Propulsion Laboratory. *Modeling of Nonlinear Combustion Instability in Solid Propellant Rocket Motors*, by J. D. Baum and J. N. Levine. Edwards Air Force Base, California, February 1984. (AFRPL-TR-83-058, publication UNCLASSIFIED.)
20. Air Force Rocket Propulsion Laboratory. *Nonlinear Analysis of Solid Rocket Combustion Instability*, by J. N. Levine and F. E. C. Culick. Edwards Air Force Base, California, October 1974. (AFRPL-TR-74-45, publication UNCLASSIFIED.)
21. P. G. Harris and A. Champlain. "A New Methodology for the Analysis of Experimental Data Describing Pulse-Triggered Nonlinear Instability in Solid Rocket Motors," AIAA Paper 98-3558 (July 1998).

INITIAL DISTRIBUTION

- 1 Naval Air Systems Command
AIR 4.0T3, Scott Shumway
- 1 Office of Naval Research, Washington, DC (Code 333, Judah Goldwasser)
- 1 Naval Postgraduate School, Monterey, CA (Department of Aeronautical & Astronautical Engineering, Dave Netzer)
- 1 Air Force Office of Scientific Research (AFOSR), Washington, DC, (Mitat Birkan)
- 1 Air Force Research Laboratory, Edwards AFB, CA (AFRL/PRSA Department, Jay Levine)
- 2 National Aeronautics Space Administration, Marshall Space Flight Center, Huntsville, AL
EP-54, Charles Martin (1)
ED-32, Tom Nesman (1)
- 1 Aerojet Propulsion Company, Sacramento, CA (Randell Peeters)
- 1 Aerospace Corporation, Los Angeles, CA (Kirsten Pace)
- 4 Alliant Techsystems, Magna, UT
Tim Bruce (1)
Garn Butcher (1)
Scott Cunningham (1)
Richard Raun (1)
- 2 Alliant Techsystems, Rocket Center, WV
Marty Harsh (1)
Kenneth Hartman (1)
- 1 Brigham Young University, Provo, Utah
Department of Chemical Engineering, (Merrill Beckstead)
- 1 Brown Associates, Inc., Santa Clara, CA (Robert Brown)
- 1 California Institute of Technology, Pasadena, CA (Fred Culick)
- 1 Caveny, Ft. Washington, MD (Lenard Caveny)
- 1 Chemical Propulsion Information Agency, Columbia, MD (Mary Gannaway)
- 1 Cohen Professional Services, Redlands, CA (Norman Cohen)
- 2 Defense Technical Information Center, Alexandria, VA
- 1 ERC, Incorporated, Huntsville, AL (Propulsion Analysis Department, Harold Whitesides)
- 1 Flanagan, Stanwood, WA (Joseph Flanagan)
- 1 Geisler Enterprises, Tehachapi, CA (Robert Geisler)
- 1 Hessler, Somerville, AL (Richard Hessler)
- 1 National Ground Intelligence Center
Military Technologies Division, C. Beiter (1)
- 4 Pennsylvania State University, University Park, PA
Department of Mechanical Engineering, Kenneth Kuo (1)
Department of Mechanical Engineering, Thomas Litzinger (1)
Department of Aerospace Engineering, Mike Micci (1)
Department of Mechanical Engineering, Vigor Yang (1)
- 3 Pratt and Whitney, Propulsion Division, San Jose, CA
Jeff Freeman (1)
Chuck Shaeffer (1)
Herb Wayland (1)
- 1 Science Applications International Corporation (SAIC), Gainesville, VA, (Woody Waesche)
- 1 SEA Inc., Carson City, NV (Douglas Coats)

- 1 Stone Engineering, Huntsville, AL (W. Stone)
- 4 Thiokol Corporation, Brigham City, UT
 - Research and Development Laboratories, Carol Campbell (1)
 - Al Drendel (1)
 - Joni Endicott (1)
 - Kile Speas (1)
- 1 Thiokol, Elkton, MD (DLV Operations, David McGrath)
- 1 United Technologies Research Center, East Hartford, CT (Physical & Mathematical Modeling Department, Jayant Sabnis)
- 1 University of Alabama, Huntsville (Mechanical Engineering Department, Robert Frederick)
- 1 University of Cincinnati, Cincinnati, OH (Mechanical Engineering School, Effie Gutmark)
- 1 University of Delaware – Newark (Department of Chemistry & Biochemistry, Thomas Brill)
- 4 University of Illinois, Urbana, IL
 - Department of Aeronautical and Astronautical Engineering, Robert Beddini (1)
 - Department of Computational Science and Engineering, Michael Heath (1)
 - Department of Mechanical Engineering, Herman Krier (1)
 - Department of Mechanical Engineering, Quinn Brewster (1)
- 1 University of Utah, Salt Lake City, UT (Department of Chemistry, Chuck Wight)

ON-SITE DISTRIBUTION

- 1 Code 477000D (S. Blashill)
- 2 Code 477100D (V. Hart, G. Sieg)
- 3 Code 477200D (J. Baldwin, J. Braun, D. Ciaramitaro)
- 4 Code 477300D (J. Barkman, J. Gross, J. Kapeles, J. Kong)
- 2 Code 477400D (J. Bratcher, C. Toftner)
- 2 Code 477B00D (F. Pickett, R. Toftner)
- 1 Code 477E00D (S. Fuller)
- 1 Code 477K00D (P. Gattis)
- 1 Code 47C000D (J. Robbins)
- 1 Code 47CA20D (P. Chun)
- 2 Code 4T1000D (F. Markarian, T. Loftus)
- 1 Code 4T4300D (T. Boggs)
- 1 Code 4T43A0D (T. Atienza-Moore)
- 2 Code 4T4310D (A. Atwood, M. Chan)
- 4 Code 4T4320D (3 plus Archives copy)
- 1 Code 528200D (J. Matson)
- 1 Code 528B00D (P. Gorish)